2021

Low Frequency Oscillations of Hemodynamic Parameters as a Novel Diagnostic Measure for Traumatic Brain Injury

Andrea Gomez Carrillo
Wright State University

LOW FREQUENCY OSCILLATIONS OF HEMODYNAMIC PARAMETERS AS A NOVEL DIAGNOSTIC MEASURE FOR TRAUMATIC BRAIN INJURY

A thesis submitted in partial fulfilment
Of the requirements for the degree of
Master of Science in Biomedical Engineering

By

ANDREA GOMEZ CARRILLO
B.S.B.E., Wright State University 2020

2021
Wright State University

WRIGHT STATE UNIVERSITY

GRADUATE SCHOOL

May 28, 2021

I HEREBY RECOMMEND THAT THE THESIS PREPARED UNDER MY SUPERVISION BY Andrea Gomez Carrillo ENTITLED Low Frequency Oscillations of Hemodynamic Parameters as a Novel Diagnostic Measure for Traumatic Brain Injury BE ACCEPTED IN PARTIAL FULFILLMENT OF THE REQUIREMENTS FOR THE DEGREE OF Master of Science in Biomedical Engineering.

_____

Ulas Sunar, PhD.
Thesis Director.

_____

Subhashini Ganapathy, PhD.
Chair, Department of Biomedical, Industrial, and Human Factors Engineering.

Committee on
Final Examination

_____

Ulas Sunar, Ph.D.

_____

Tarun Goswami, Ph.D.

_____

Brandon Foreman, MD, FACNS

_____

Barry Milligan, Ph.D.
Vice Provost for Academic Affairs
Dean of the Graduate School

ABSTRACT

Gómez-Carrillo, Andrea. M.S.B.M.E, Department of Biomedical, Industrial and Human Factors Engineering, Wright State University, 2021. *Low Frequency Oscillations of Hemodynamic Parameters as a Novel Diagnostic Measure for Traumatic Brain Injury*

There is a need to improve methods of monitoring patients with traumatic brain injury (TBI) in hospital settings. Current monitoring techniques and diagnosis methods are expensive, invasive, do not provide continuous measures, expose the patient to radiation, are ambiguous in the information they provide, and/or cannot be implemented at the bedside. These techniques measure imperative markers of brain function including intracranial pressure (ICP), cerebral blood flow (CBF), and oxygenation in the brain, among others. Hospitals not only require a practical method for real-time monitoring of patients at the bedside, but also meaningful metrics that characterize TBIs, since the variety of methods results in complex and ambiguous criteria for defining TBIs. Trends in the literature show a reliance on functional assessments such as the Glasgow Coma Scale (GCS) to define TBIs, however studies have shown its complexity and context-dependence in predicting outcome. Real-time cerebral assessment is currently focused on ICP monitoring, but increased attention to hemodynamic measures to improve patient

outcomes warrants new technologies and metrics. Therefore, in this thesis, a novel metric of low-frequency oscillations (LFOs) from hemodynamic monitoring is proposed to provide a more objective characterization of TBI. Literature suggests that these LFOs originate from the regulation of regional changes in CBF and energetic metabolism and not from systemic regulation of the cardiovascular system, making it a representative metric of brain function. Overall, this thesis will contribute to the clinical understanding of TBI through optical imaging-derived LFOs. To achieve this overall goal, the followings have been investigated between non-TBI and TBI groups: 1) quantification of absolute concentration changes of hemodynamic parameters, 2) assessment of the LFO spectrums of the oxygenated hemoglobin signals to identify prevalent LFOs, and finally 3) quantification of the average power in predefined LFO slow bands. The results indicate that optical imaging can provide noninvasive neurovascular biomarkers for continuous assessment of TBI patients.

Table of Contents

List of Figures

List of Tables

Abbreviation's List

TBI	Traumatic Brain Injury
ICP	Intracranial Pressure
CBF	Cerebral Blood Flow
GCS	Glasgow Coma Scale
LFO	Low Frequency Oscillation
fNIRS	Functional Near Infrared Spectroscopy
ASD	Autism Spectrum Disorder
TD	Typically Developing
CDC	Centers for Disease Control
CT	Computed Tomography
MRI	Magnetic Resonance Imaging
SPECT	Single Photon Emission Computerized Tomography
PET	Positron Emission Tomography
DCI	Delayed Cerebral Ischemia
CPP	Cerebral Perfusion Pressure
HOB	Head Of Bed
BOLD	Blood Oxygen Level Dependent
PO_2	Brain Tissue Oxygen Tension
CA	Cerebral Autoregulation
fMRI	Functional Magnetic Resonance Imaging
SWI	Susceptibility Weighted Imaging
CMB	Cerebral Microbleed
MPI	Magnetic Particle Imaging
US	Ultrasound
GFAP	Glial Fibrillary Acidic Protein
TRACK-TBI	Transforming Research and Clinical Knowledge in Traumatic Brain Injury
CRP	C-Reactive Protein
EEG	Electroencephalography
SvO_2	Cerebral Oxygen Saturation
OV	Oxygen Variability
MAP	Mean Arterial Pressure
PMT	Photomultiplier Tube
DPFC	Dorsolateral Prefrontal Cortex
HUT	Head-Up-Tilt
NIR	Near Infrared Region
DC	Direct Current
AC	Alternating Current

R_i	Source-Detector Separstion
DCCF	Direct Current Correlation Factor
OD	Optical Density
DPF	Differential Pathlength Factor
MBLL	Modified Beer-Lambert Law
PSD	Power Spectral Density
FFT	Fast Fourier Transform
f_s	Sampling Frequency
CBFV	Cerebral Blood Flow Velocity
API	Average Percent Increase
APD	Average Percent Decrease
HBO	Oxygenated Hemoglobin
HB	Deoxygenated Hemoglobin
*[*HBO*]*	Oxygenated Hemoglobin Concentration
[HB]	Deoxygenated Hemoglobin Concentration
[THC]	Total hemoglobin Concentration
μ_a	Absorption Coefficient
μ_s’	Scattering Coefficient
ε	Extinction Coefficient
CW	Continuous Wave
FD	Frequency Domain
SNR	Signal-to-Noise Ratio

Acknowledgment

I would like to express my gratitude to the WSU Biomedical Imaging Lab for providing me this opportunity and continuous support throughout this project. From the beginning, my advisor, Dr. Ulas Sunar, expressed a desire to see me create meaningful work in an area that interested me and would have a significant impact. Thank you for teaching, supporting, and encouraging me as I navigated this project that combined the exciting fields of medicine, athletics, and biomedical optics.

I would be remiss not to mention the invaluable help I received from members of the lab. Thank you to Alex Bergen for introducing me to the instruments and technologies in the lab. Thank you to Dharminder Langri for answering all of my questions and helping me with suggestions on instrument setup. Finally, thank you to Benjamin Rinehart for the continuous support with theory, signal processing, and protocol suggestions. You have all been valuable mentors and great friends.

To other members of Wright State, thank you for your advice and suggestions. To Mike Bottomley and Yan Su, thank you for your suggestions regarding statistical analysis. To Phil Flynn, thank you for your guidance to helpful resources for my literature review.

To my family and friends, I am forever grateful for your support. Thank you to my parents Laura and Abel for always encouraging me and providing unconditional support. Thank you to my brothers Dani and Mau for reminding me to just keep swimming. Thank you to my aunt, cousins, and grandfather Victor Carrillo for being a source of inspiration. And finally, thank you to my friend Maddie Jewell for her strength, courage, and perseverance despite adversity that inspired this thesis.

1. Introduction/Motivation

This section will provide the motivation behind this thesis. It includes a thorough overview of TBI that highlights its prevalence and gaps in practical methods of its diagnosis and management. It includes a summary of functional near infrared spectroscopy (fNIRS) and its uses in the field, and finally it introduces low frequency oscillations (LFOs) as a potential novel metric for TBI assessment. I conclude this section with the implications of this project and its clinical significance.

1.1. Traumatic Brain Injuries

Traumatic brain injuries (TBIs) have been in conversation for a few centuries with relevant literature dating back to 1891[5]. A TBI is defined as a blow or jolt to the head, which can disrupt the function of the brain[6]. Numerous events can lead to such damage, including mechanical falls, traffic accidents; military combat injuries, and sports injuries among others. Overall, there is a complicated variation in criteria and terminology when assessing TBIs[7], and the current modalities are not optimal for continuous real-time monitoring or are invasive and place an already vulnerable brain at risk.

Various disciplines have examined this widespread health concern including nursing [6], biomechanical/sports research [8–13], pediatrics [14–16], army studies [17], surgery [18], rehabilitation [19,20], and neuropsychology/psychiatry [21–24], with an emergence in engineering [25–31] among others. Articles, studies, and reviews assess TBIs from multiple angles. From epidemiology [10,32–35], to etiology, to potential biomarkers for diagnosis [12,36–40], various treatment approaches [41–47], and even studies that assess the correlation between

player position in football and the risk of TBI[13], the variety of perspectives surrounding this topic corresponds to the complexity of addressing it clinically.

While in the 1990s the push was for more helmet use to prevent head injuries after serious bicycle accidents[48], and more recently the concern is to increase the surveillance of TBI in youth sports [11], whatever the cause is, the prevalence of TBIs remains concerning. Trauma is the third leading cause of death worldwide, just trailing cerebrovascular disease and cancer[49]. TBIs contribute greatly to trauma-related deaths and disabilities, accounting for almost one-third of injury-related deaths[50]. In the United States, 5.3 million people are estimated to live with long-term disabilities due to TBIs, a figure that underrepresents the injury's incidence due to lack of reporting and diagnoses[51]. In China, where brain-monitoring methods are not readily available[5], there is also a high prevalence of TBI[2]. A study on a brigade combat team accentuates the prevalence as researchers found that roughly 23% of soldiers return with a TBI[17]. Not only is this issue rampant in numerous contexts, but the ambiguity in assessing the human brain due to its highly individualized nature also becomes problematic in diagnosing TBI. A study on the accuracy of mild TBI diagnosis showed that 56% of patients who met the TBI criteria from the Centers for Disease Control and Prevention (CDC) were not diagnosed by the emergency department[2]. This means over half of the patients suffering from brain injury walked out of hospitals unknowing of their condition. A phenomenon known as secondary brain injury makes this a problematic statistic since impeded CBF due to the initial impact continues to damage the brain post-trauma. Therefore, diagnosing the brain becomes crucial, but current diagnostic methods are limited to self-reporting symptoms, functional assessments such as the GCS, speech tests, language tests, cognition

assessments, and neurophysiological tests. Occasionally, computed tomography (CT) scans, magnetic resonance imaging (MRI), single-photon emission computerized tomography (SPECT), or positron emission tomography (PET) are used to detect brain bleeds and damaged tissue, but such techniques are not suited for long-term use and might not even be ordered by physicians. Numerous studies acknowledge the consequences of secondary brain injury, which increase the mortality from 10 to 56%[53], emphasizing that treatment should focus on preventing it. A recent review on TBI advances outlines common treatments including anti-seizure prophylaxis, decompressive craniectomy, hyperosmolar therapy, targeted temperature modulation to prevent hyperthermia, and/or ICP monitoring[43, 45]. ICP monitoring is a recurring theme in the literature and is arguably the most routine medical observation employed for TBI patients. In an international survey of neurointensivists on the current practices of neuromonitoring, they found that ICP monitors were the most available tool and the most commonly used variable for the management of delayed cerebral ischemia (DCI), a potential secondary brain injury[54]. Numerous articles over the past decades stress the need for continuous monitoring to prevent secondary injury[53,55–57], with managing ICP and cerebral perfusion pressure (CPP) a main focus[41–43,46,47,58]. However, there is disagreement on whether ICP or CPP-based management best benefits patients, warranting more research on the management of TBI. Methods to manage pressure parameters such as these are also inconsistent across hospitals, further complicating consensus on optimal patient care. Feldman first validated elevating the head-of-bed (HOB) of patients as one such method in 1992 in a study where he found a 30-degree elevation to be optimal in reducing ICP while maintaining CPP and CBF[59]. This was later confirmed in a practice

audit by Schulz-Stübner et al.[60] making this elevation standard positioning for ICP management. However, recent studies in the pediatric population suggest that an optimal elevation is not limited to 30-degrees and should be individualized to patients[61]. While there are several other means of managing ICP including IV solutions, hyperventilation, and surgical interventions[62], other comorbidities of TBI deserve attention. One concern is cerebral ischemia, which requires both CBF and oxygenation-based monitoring. A study published in the Journal of Neurosurgery strengthens the need for additional metrics to improve patient outcomes, as ICP/CPP management does not always prevent ischemia. In the study, they found that adding brain tissue oxygen tension (PO_2) monitoring to traditional ICP monitoring reduced the mortality rate from 44 to 25%[63]. This is important because it stresses the need to guide therapy with tissue oxygenation in addition to pressure measures that are already in practice. Emerging protocols for TBI management, especially in severe scenarios, combine both oxygenation and ICP measures to decide the course of treatment. A recent article from the Seattle International Severe Traumatic Brain Injury Consensus Conference is even attempting to develop an algorithm that guides individualized treatment for patients with increased ICP but normal PO_2, or patients with normal ICP but decreased PO_2[47]. Recent attention to the combination of oxygenation and pressure measures directs our focus to advance oxygenation and CBF monitoring methods in hospital settings.

The assessment of CBF in TBI subjects can be traced back to 1978 in a study of cerebral autoregulation (CA) of unconscious patients[64]. In the study, they utilized the intra-arterial 133xenon washout method to measure rCBF and found regional autoregulation loss in most studies[64]. This outdated method, however, requires local

injection of xenon and was proven unreliable in later assesments[65]. The need for reliable hemodynamic monitoring of TBI patients is where the previously mentioned modalities of CT/PET/SPECT scans and MRIs can take snapshots of the brain and detect bleeds, but do not provide the continuous feedback physicians need to identify deteriorating conditions. Additionally, avoiding patient and physician exposure to radiation is a widespread medical consensus, and the push away from CT is even strengthened by a recent study showing that fast brain MRIs outperform them in specificity, sensitivity, and negative predictive value of TBI diagnosis[14]. Regarding the disadvantages of PET and SPECT, they both need a long measurement period to detect accumulated hemodynamic changes and have low temporal and spatial resolution[66]. The historical alternative to provide continuous monitoring has been functional MRI (fMRI), but it is limited to 1-2 hours of recording and is not ideal for the bedside. An MRI sequence of susceptibility-weighted imaging (SWI) has recently been proposed to detect cerebral micro bleeds (CMBs) prevalent in TBIs that are undetectable in normal MRI and CT scans. Researchers in the medical imaging field are investigating machine/deep-learning methods using 3D-convolution neural networks to detect these tiny bleeds[67], but it is still a relatively new topic and beyond the scope of this thesis. Another emerging, radiation-free technology of magnetic particle imaging (MPI) for real-time perfusion monitoring proves advantageous over these large machines in practicality, efficiency, and temporal resolution and has been validated by MRI in mice studies[68]. The first in vivo study of TBI patients also showed excellent contrast in showing changes in blood pool over time[69], however there is concern of the effects of time-varying magnetic fields on nerve stimulation and even allergic reactions to the administered iron oxide nanoparticles have

been reported[70]. MRI, MPI, SPECT, and PET modalities are also costly, therefore limiting their use and posing a concern for underfunded healthcare settings where there is not access to such technologies. Another method that has existed for over 50 years is jugular venous oximetry, where fiber optic oximetry catheters are inserted into the jugular bulb[71], but it is invasive and rarely used[72]. Transcranial Ultrasound (US) Doppler imaging has also been proposed as a more cost-effective and portable means of quantifying blood flow velocity, which has been related to assessing cerebral autoregulation and even corresponding ICP[27], however its accuracy in this latter relationship is in question[73,74]. The technique is also limited for longitudinal monitoring because of relatively bulky US transducers, which make it hard to position the US probe on the scalp. Thus, there is a need for a more practical method of continuously monitoring of brain hemodynamics to manage TBI and is the focus of this thesis research. For this overall goal, fNIRS technology is used for hemodynamic monitoring and novel LFO analysis. FNIRS is noninvasive, safe, low-cost, portable, convenient for bedside settings, does not require immobilization of the patient, has continuous monitoring capabilities, and has high temporal and adequate spatial resolution[75]. Finally, it has reliable data that has been proven by PET and fMRI[76].

1.2. Functional Near Infrared Spectroscopy

Functional near-infrared spectroscopy (fNIRS) has been in conversation since the late 1900s, notably beginning with a study on hemoglobin using a ‘Cary 14’ spectrophotometer to begin understanding hemoglobin’s oxygen affinity characteristics[79]. Since then, it has expanded from a simple noninvasive method of measuring oxygen in

tissues of cats[80] to an enormous variety of applications. An optical imaging modality, fNIRS, detects changes in the concentration of oxygenated (HbO) and deoxygenated (Hb) hemoglobin as a means of assessing cerebral activity. Using a dual-wavelength light emitter and photodetector, it can calculate blood volume and estimate local oxygenation changes, with additional emerging capabilities in the field of TBI. In the medical field, its applications have ranged from muscle studies including tissue oxygenation during exercise, metabolic myopathy, and effects of lung diseases on muscle[83–88], to cancer-characterization studies including skin[89], prostate[90] and breast cancer[91,92], and even to type-I and type-II diabetes as a noninvasive glucose-monitoring modality beginning in 1992[93–97]. The variety of applications of fNIRS showcases its potential as an established technology. For our purposes, we are interested in using it for neuromonitoring. Its use in cerebral studies dates back to the late 1900s with investigations on neurological diseases such as schizophrenia[98–102] and Alzheimer's disease[103,104]. In the early 2000s studies incorporated migraine[105], brain edema[106], and optic neuritis[107]. Task-related research also began to surface as studies evaluated brain function during attention impairments[23], cognitive rehabilitation[20], and mental fatigue assessments[22]. The complexity-task initially assessed by fNIRS in 2012[28] even evolved into developing machine-learning biomarkers of TBI as spatio-temporal features proved to be characteristic of brain injuries[29]. This successful use of fNIRS to characterize TBIs affirms our selection of this technology for our project, although not in the same manner. In fact, fNIRS has been finding its place particularly in infant brain studies partially due to its ability to handle motion artifacts and higher light penetration depth in the infant brain. More recent and innovative investigations involve interesting neural studies of

OCD[21], hemodynamic evaluation of trust in the only-child effect[24], and even findings of decreased cerebral oxygenation during mental tasks in subjects with type 2 diabetes[108]. The portability of fNIRS technology also allows it to be used in agricultural technology, army and sport settings, and it has even been found that it could induce an immune response to vaccines and be utilized in doctors' offices[109]. Albeit compelling, these recent applications of fNIRS are outside the domain of our project.

With the first fNIRS infant brain study dating back to 1998[110] that assessed regional hemodynamic responses to visual stimuli in awake infants, there have been over thirty infant-related studies since[111]. Fox's review on fNIRS-based infant studies provides an adequate representation on the current signal processing methods used to derive meaningful information from temporal light intensity changes that eventually give hemodynamic information. They note that signal processing generally begins with low-pass filtering to correct linear trends, and then the Beer-Lambert law relates intensity changes to concentration changes of HbO and Hb—with HbO generally accepted as the preferred measure of cortical activation. This is applicable to our project as cortical activation is of interest in patients with potential secondary brain injury. Regarding TBIs specifically, studies show a decrease in HbO than normal due to cognitive impairment. In a study comparing TBI subjects to healthy controls when receiving targeted and context stimuli, significant decreases were found in the hemodynamic response between the two, with reduced amplitude in the TBI group[23]. Another study found a higher increase in HbO, Hb, and THC in TBI patients with head lowering when compared to healthy patients[145]. This shows both the potential of fNIRS parameters and manipulating the head of a patient's bed to differentiate healthy and diseased states, which is the premise of this

project. As previously mentioned, monitoring brain tissue oxygenation is crucial for TBI management—making fNIRS ideal in clinical use. Its lack of use in hospitals[112,113], therefore, warrants questioning—especially since the reliability of fNIRS to provide continuous hemodynamic data has been extensively validated over the years by fMRI[114] and has been well established for research purposes. TBI does bring some complications to traditional fNIRS monitoring with interference from the scalp[115] that is exacerbated by stress responses from the TBI itself, and the presence of hematomas that can misrepresent cerebral hemodynamics[116]. A review on the use of NIRS in TBI concludes that it is mostly used in the identification of hematomas, but the reliance largely remains on ICP monitoring for TBI management as the relationship of hemodynamics and targeted therapy is not well-understood yet[116]. Some studies have shown a potential relationship between ICP and NIRS parameters, but it is not sufficient yet to contend that fNIRS should be utilized in clinical settings[117,118].

We still believe there is great benefit in incorporating fNIRS to hospital bedside monitoring and seek to reinforce the strengths of this technology by going beyond the traditional time-series processing and reconstruction of functional images[119] to new metrics that can better characterize TBI. New signal processing methods in the frequency domain (FD) are being experimented, with Welch's method playing a key role in estimating power spectrums. Recently, Welch's method was used to process fNIRS signals and successfully detect spontaneous frequency changes in deceptive behavior[120]. We are proposing applying this type of frequency analysis to further the knowledge of TBI characterization with new metrics.

1.3. Low Frequency Oscillations

Frequency analysis of the brain is not a novel idea as electrical studies of the cortex of rats date back to the mid 1900s[121]. Historically, it seems electroencephalography (EEG) has been the dominant technique for assessing cerebral oscillations. The frequency at which neurons fire in the brain has been widely shown to be representative of brain function[122] with five commonly categorized bands: delta (0.5–4 Hz), theta (4–8 Hz), alpha (8–12 Hz), beta (12–30 Hz) and gamma (>30 Hz)[123]. Lower frequencies, however, are only recently appearing in the literature as potential biomarkers of TBI. It is thought that lower frequency oscillations (LFOs) may represent the regulation of changes in rCBF and energetic metabolism rather than systemic regulation of the cardiovascular system[4]. Additionally, numerous studies support that LFOs in the 0.07-0.1 Hz range can be linked to CA[124–126]. These beliefs are exciting as they show the potential of directing research at LFOs characterizing TBIs. While an EEG study on thalamocortical oscillations in sleep and arousal from 1993 acknowledges the potential value of frequencies less than 1 Hz[127], and another study in Russia from 1988 recognized EEG frequencies of 0.2-2Hz in patients with ablation of tumor surgery[128], not many studies have investigated these faster oscillations in the brain. LFO investigation through EEG-technology has recently emerged in migraine studies where they define four characteristic bands of spontaneous oscillation: slow-5 (0.01–0.027 Hz), slow-4 (0.027–0.073 Hz), slow-3 (0.073–0.198 Hz) and slow-2 (0.198–0.25 Hz) and found an abnormal presence of these LFOs in the thalamus associated with headache attacks[129]. Although the use of EEG to investigate LFOs is relatively new, fMRI actually exists in LFO-related literature as early as 1995, showing that the idea of fast hemodynamic oscillations might have been around longer

than the lack of the presence of these metrics make it seem. In an early study, resting fMRI showed that fluctuations lower than 0.1 Hz correlate with motor function and may show the functional connectivity of the brain[130]. Other studies using the blood-oxygen level dependent (BOLD) signal from fMRI also agree that ~0.08-0.1 Hz LFOs are an intrinsic property of the brain that may modulate the well-known higher frequency activity and play an important role in brain organization[131–134]. More recent uses of fMRI include findings of LFO activity in the hippocampus representative of sensory information integration[135], and an interesting study was able to localize affected areas of lower back pain in the brain from altered amplitudes of LFOs[136]. Furthermore, two different studies on patients with retinal vein occlusion and non-neuropsychiatric systemic lupus erythematous found LFO amplitude changes in multiple brain regions[137,138]. This also showcases the strength of fMRI LFO-assessment in providing a spatial discovery of neural mechanisms of diseases. Its application to TBI was introduced in an fMRI study that found differences from healthy controls in the slow-4 and slow-5 frequency band amplitudes in occipital areas of the brain[139]. MRI, however, is limited to only assessing Hb[140] and with the limitations of fMRI previously mentioned, fNIRS presents a practical alternative to LFO analysis. The first CBF LFOs were found in Kato's study from 2013 where 0.06-0.1 Hz oscillations in NIRS parameters were representative of resting state brain function. In this study, they found increased LFOs in preterm infants than term infants, suggesting an inverse correlation between LFOs and brain function[16]. While this was the first use of NIRS parameters to define LFOs, a study from 2008 used NIRS-based LFOs to calculate an estimate of cerebral oxygen saturation (SvO2) that was validated by an intraparenchymal catheter[141].

The fact that this novel metric is already being validated as a means of estimating more parameters adds to its potential as a future metric of TBI. A previously mentioned study attempting to add machine-learning to identify biomarkers of TBI also looked into LFOs from the HbO signal ranging from 0.01-0.1 Hz as characteristic of the disease during a complexity task. They found this frequency feature was able discriminate between TBI and healthy populations[29], which is promising for this project's analysis. An additional biomarker arising from LFO analysis measured by fNIRS is the oxygen variability (OV) index. Its ability to characterize TBI was validated in Chernomordik's study comparing cognitive load between brain-injured subjects and healthy controls[140].

Another optical technology worth mentioning that has been applied to LFO detection is with a Nikon epifluorescence microscope. In the study, they found dominant frequencies of oscillations between 0.039 and 0.078 Hz in the cerebral cortex of a tottering mouse to assess the neural events of dystonia[142]. This is interesting since these are similar (the) frequencies of interest recently found in TBI LFO studies. As promising as these studies are, they are scarce and TBI-related LFO analysis needs more research to demonstrate itself in the field. With the need for a standardized method of continuous real-time brain data, we present studying LFOs in TBI subjects undergoing a HOB elevation change. HOB elevation manipulation has already been explained as a means of managing TBI by lowering ICP while maintaining CPP.

1.4. Implications of this Project

We propose merging these numerous innovative insights and technologies surrounding TBI to contribute meaningful knowledge to the field. By utilizing a fNIRS probe to measure HbO and Hb as subjects undergo HOB elevation changes, we hope to provide an

understanding of CA differences between TBI and healthy subjects. We plan to base our protocol on Cheng's assessment of healthy subjects undergoing a 70 degree elevation change that was able to quantify CA by assessing phase shifts between the LFOs of mean arterial pressure (MAP) and hemodynamic parameters[30]. While confident in their results, they acknowledge the need to expand their study to subjects with cerebral impairment, which is where this thesis project fills in by characterizing the cerebral response of a non-TBI and a TBI population undergoing HOB elevation changes using FD analysis of the fNIRS signal. First, the frequencies of interest are identified, then LFO spectrums of each study group are compared, and finally HOB of elevation changes on the LFO slow-bands are quantified. In a broader impact, it is expected that this study demonstrates the potential of fNIRS-LFO technology to assess brain injuries and diseases using a practical HOB protocol, and to prompt future studies to eventually validate its use in hospital settings.

2. Materials and Methods

This section will outline the methods used in this project. We will include an overview of participating subjects, the HOB manipulation protocol, theory behind optical instrumentation and signal processing in the time and frequency domains.

2.1. Subjects

In total, this project utilized fifteen volunteers from Wright State University with mean age of 23.8 years, range of 20-40 years. There were 7 males and 6 females of which one female met the criteria of a TBI from a Glasgow coma score of 15 by their respective athletic trainers. Due to the small sample size of TBI subjects, the sole TBI subject underwent three measurements for a total of three recordings for the TBI population. For the healthy population, each subject underwent one measurement. Two healthy subjects, however, were excluded due to motion artifacts during their measurements resulting in twelve recordings for the healthy population. The remaining participants had a mean age of 25.5 years and a range of 20-40 years. Both populations, TBI and healthy, underwent the same ten-minute measurement protocol after a five-minute baseline stabilization period where no measurements took place. The International Review Board of Wright State University approved this protocol and participants consented to the measurements.

2.2. fNIRS System

This project used the fNIRS system (OxiplexTS™ instrument from ISS) to measure HbO and Hb concentrations in tissue. The sensor of this fNIRS system consists

of eight laser diode sources and a photomultiplier tube (PMT) as a detector. This 8-channel array sits in a black polyutherane rubber sensor with a side entry for the fibers, adding flexibility to the design[143]. Source-detector pairs are 1.5, 2.0, 2.5, 3.0 cm apart, and an average optical power of less than 1 mW makes the device comply with ANSI safety standards. It works in the FD by modulating NIR light at 110 MHz into tissue at two different wavelengths (830 nm and 690 nm) and exporting the collected signal as an ASCII file that is processed in MATLAB 2018b. Light information traverses through a microprocessor and sends the signal to the computer as intensities through a USB cable. With the assumption that hemoglobin acts as the main absorber, the instrument can uniquely determine absorption and scattering coefficients, and thus calculate HbO and Hb concentrations[143]. **Figure 1** below shows the main components of the system.

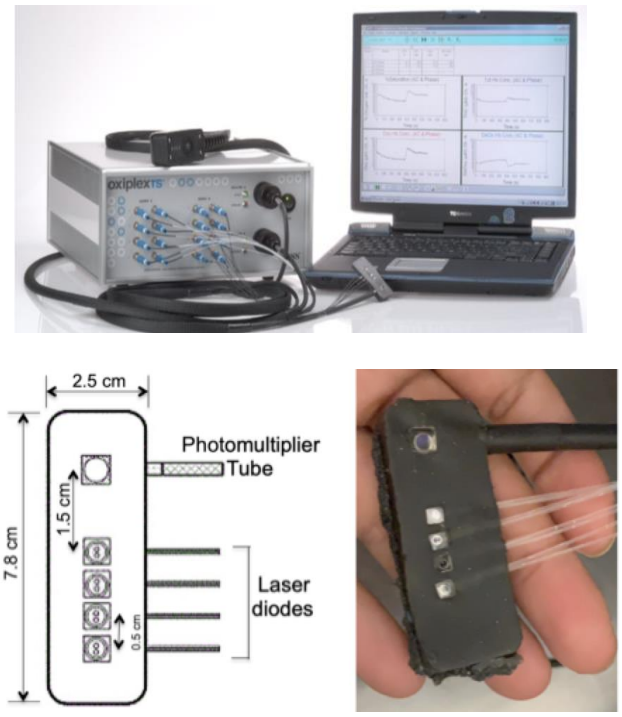

FIGURE 1: (Top) The Oxiplex TS system with fibers providing connection to the sensor and a USB cable communicating with the computer[143]. (Bottom) A schematic detailing the dimensions of the optical probe that holds the fibers[143] with the actual probe pictured on the right.

2.3. Head-of-Bed Protocol

Each subject underwent the same 15-minute HOB protocol. Subjects received explanation of study procedures and provided consent prior to beginning the measurements. The sensor was placed on the left side of the dorsolateral prefrontal cortex (DPFC) as shown in **Figure 2** below. To properly place the sensor, an EEG cap was used with markings that referenced the international EEG 10-20 system as shown in **Figure 2** below.

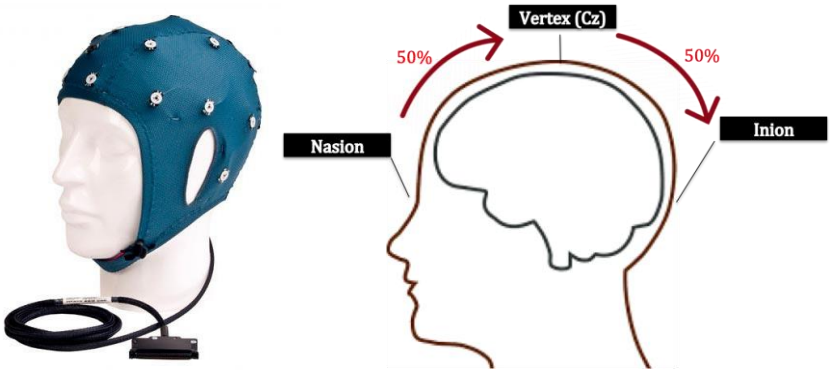

FIGURE 2: (Left) Example of EEG cap used to guide marking of Fp1 position. (Right) Diagram describing the location of the nasion and inion used to guide the EEG cap placement on the vertex of each subject.

The cap placement was then guided the source and detector locations. To properly place the cap, the distance from each subject's nasion to inion was measured with tape.

The Cz position on the cap was then placed at the halfway mark of this distance and the cap was adjusted to symmetrically fit on the subject's head. A small marking was placed slightly above the subject's left Fp1 position to guide the sensor placement once the cap was removed. The sensor's source optode was then placed on the Fp1 position (slightly below the marking) so that the marking would not interfere with the signal and the entire sensor was secured using a black elastic band around the subject's head. Final placement is visible in **Figure 3** below.

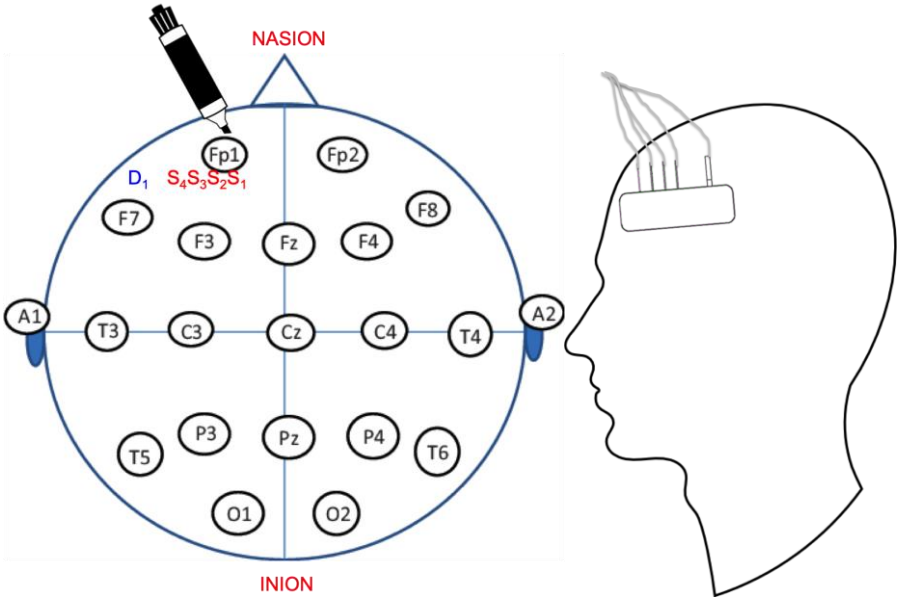

FIGURE 3: (Left) Location of marking on the Fp1 position from the International 10-20 system and the placement of detectors and sources. (Right) Location of sensor on subject's left dorsolateral prefrontal cortex.

The elevation changes in this project were facilitated using the HILL-ROM 1105 Advance Hospital Bed from Piedmont Medical Incorporated as shown in **Figure 4**. The electric bed features side rail controls that adjusted the angle of elevation of the headboard. The footboard could also be manipulated but was not used in this project.

FIGURE 4: HILL-ROM 1105 Advance Hospital Bed used for elevation changes during measurements.

Once the sensor was properly placed, subjects were asked to sit in the thick foam mattress of the bed at the initial 30-degree elevated position and relax for five minutes. After this five-minute relaxation period that established baseline conditions, the fNIRS system started a five-minute head-up-tilt (HUT) recording. The bed was then lowered to a

zero-degree angle at a rate of 2.5 degrees per second and recording continued for five more minutes. **Figure 5** below outlines the three phases of this protocol.

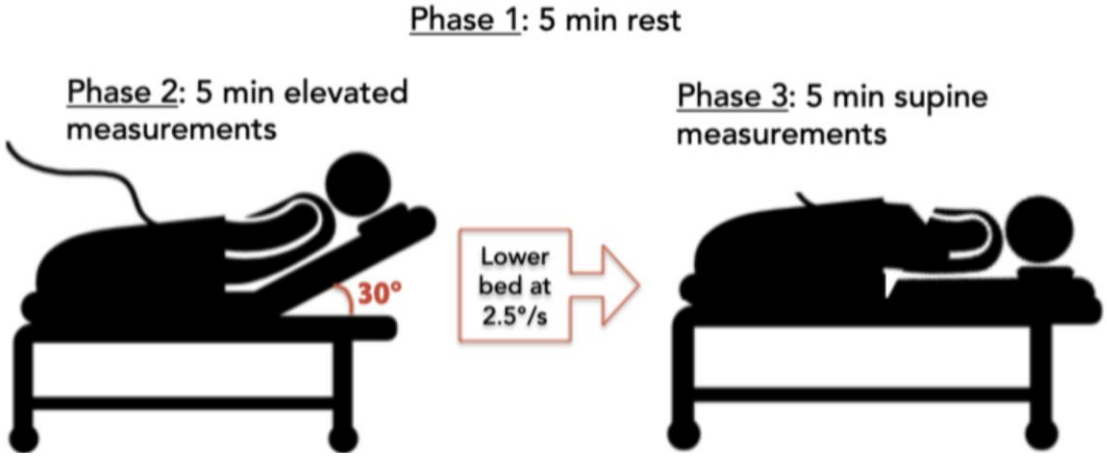

FIGURE 5: The three phases of the HOB protocol: Phase 1 was baseline establishment as the subjects rested in an elevated position, phase 2 measurements began at the elevated position for 5 minutes, phase 3 measurements continued at the resting supine position for five minutes.

2.4. FNIRS Theory

One can determine concentration changes of oxygenated and deoxygenated hemoglobin from light received by a detector because human tissue absorption is mainly due to hemoglobin in the blood at the near infrared wavelengths [650 nm-900 nm]. **Figure 6** below shows the most probable paths photons take for given source and detector configurations.

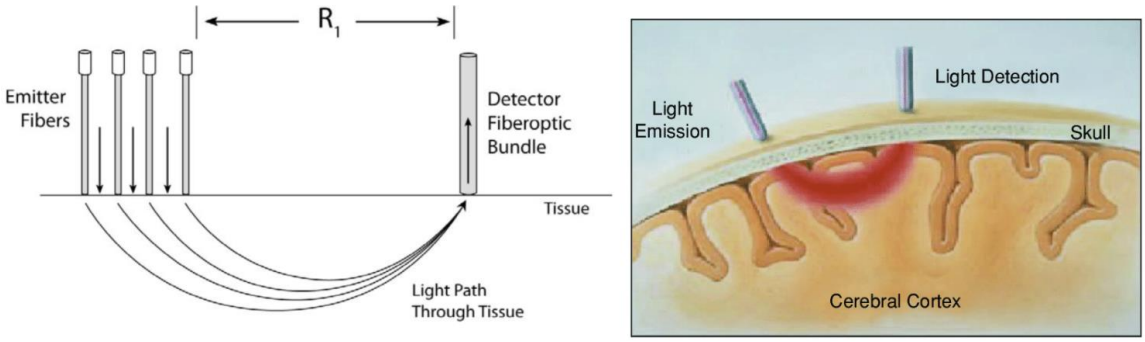

FIGURE 6: (Left) The diagram shows path of light from 4 emitter fibers to the detector on the Imagent sensor used in this project[143]. (Right) The banana shape of how light diffuses through the scalp, skull, and cerebral cortex before returning to the detector.

Photons emitted from the diodes propagate through the scalp, skull, and brain tissue. This photon propagation is mainly governed by photon diffusion, dominated by the light scattering, which allows photons to propagate deep into the tissue. Most of the photon paths from source to detector follow banana-shaped paths, as seen in **Figure 6.** Some of the photons are absorbed by the tissue chromophores. Chromophores are physiological substances that absorb light. In brain tissue, the main chromophores are HbO, Hb, and water in the NIR wavelength region. The absorption spectra of major absorbers can be seen in **Figure 7** below.

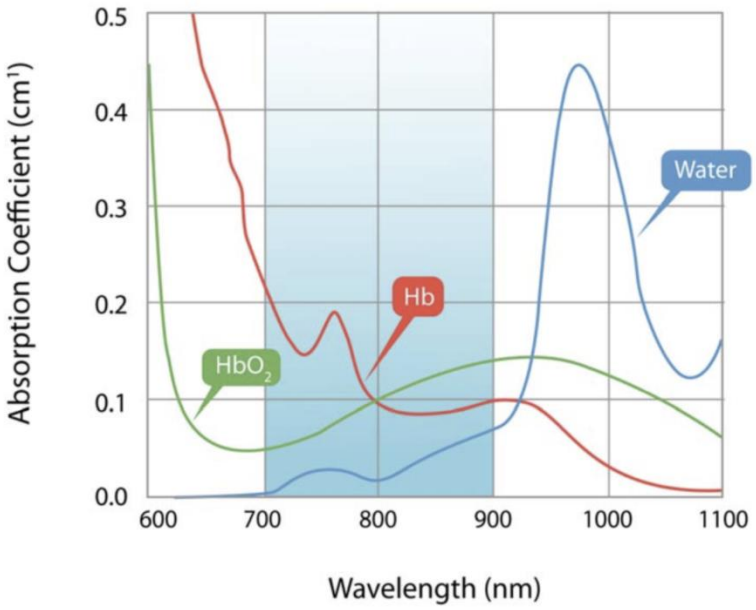

FIGURE 7: Absorption spectrum of HbO, Hb, and water with the optical window highlighted in blue[143].

The two wavelengths used in this optical technique are chosen because of the differences between the absorption properties (or extinction coefficient (ε)) of HbO and Hb and the minimal absorption of water. This contrast allows for differentiation between the two chromophores more accurately. The first wavelength used, 690 nm, is in a region where absorption for Hb is significantly higher than HbO,

and conversely the second wavelength used, 830 nm is in a region where absorption for HbO is higher. The intensity of light received at the detectors helps define absorbance (A) through **Equation 1** below, where T is the ratio of light seen by the detector (I) to the initial incident light (Io).

$$A = -\log(T) \qquad [1]$$

Absorbance is a function of each chromophore's extinction coefficient (ε) as a product of its concentration and can be related through the absorbance coefficient, μ_a, as is shown in **Equation 2** below.

$$\mu a = \varepsilon HbO[HbO] + \varepsilon Hb[Hb] + \varepsilon H2O[H_2O] \qquad [2]$$

Extinction coefficients are established values unique to each chromophore and wavelength in units of $\mu M\ M^{-1}\ cm^{-1}$, and they can be obtained from a look-up table. The OxiplexTS system assumes water concentration is set at 70% as the background absorption, which leaves the concentrations of HbO and Hb as the only two unknown values. μ_a becomes a measurable parameter through Beer Lambert's Law shown in **Equation 3** below, and therefore detecting intensity changes at two different wavelengths allows for both concentrations to be calculated.

$$[\text{oxy-Hb}] = \frac{\varepsilon_{\text{deoxy-Hb}}(\lambda_2)[\mu_a(\lambda_1) - B(\lambda_1)] - \varepsilon_{\text{deoxy-Hb}}(\lambda_1)[\mu_a(\lambda_2) - B(\lambda_2)]}{\ln(10)[\varepsilon_{\text{deoxy-Hb}}(\lambda_2)\varepsilon_{\text{oxy-Hb}}(\lambda_1) - \varepsilon_{\text{deoxy-Hb}}(\lambda_1)\varepsilon_{\text{oxy-Hb}}(\lambda_2)]}$$

$$[\text{deoxy-Hb}] = \frac{\varepsilon_{\text{oxy-Hb}}(\lambda_1)[\mu_a(\lambda_2) - B(\lambda_2)] - \varepsilon_{\text{oxy-Hb}}(\lambda_2)[\mu_a(\lambda_1) - B(\lambda_1)]}{\ln(10)[\varepsilon_{\text{deoxy-Hb}}(\lambda_2)\varepsilon_{\text{oxy-Hb}}(\lambda_1) - \varepsilon_{\text{deoxy-Hb}}(\lambda_1)\varepsilon_{\text{oxy-Hb}}(\lambda_2)]} \qquad [3]$$

However, since photons received by the detector represent both absorbed and scattered light, a modified Beer-Lambert law (MBLL) must be used to account for the dispersion. This modified equation accounts for scattering with a scattering coefficient μ_s'. The OxiplexTS can calculate both the scattering and absorption coefficients by

using FD spectroscopy where the diodes are modulated at 110 MHz. This means incident light becomes a function of time with phase (∅), DC and AC components $Io=IDC+IAC\sin(2\pi ft-\emptyset)$. The relationship between these parameters as measurements take place can be seen in **Figure 8** below from the OxiplexTS Manual[143].

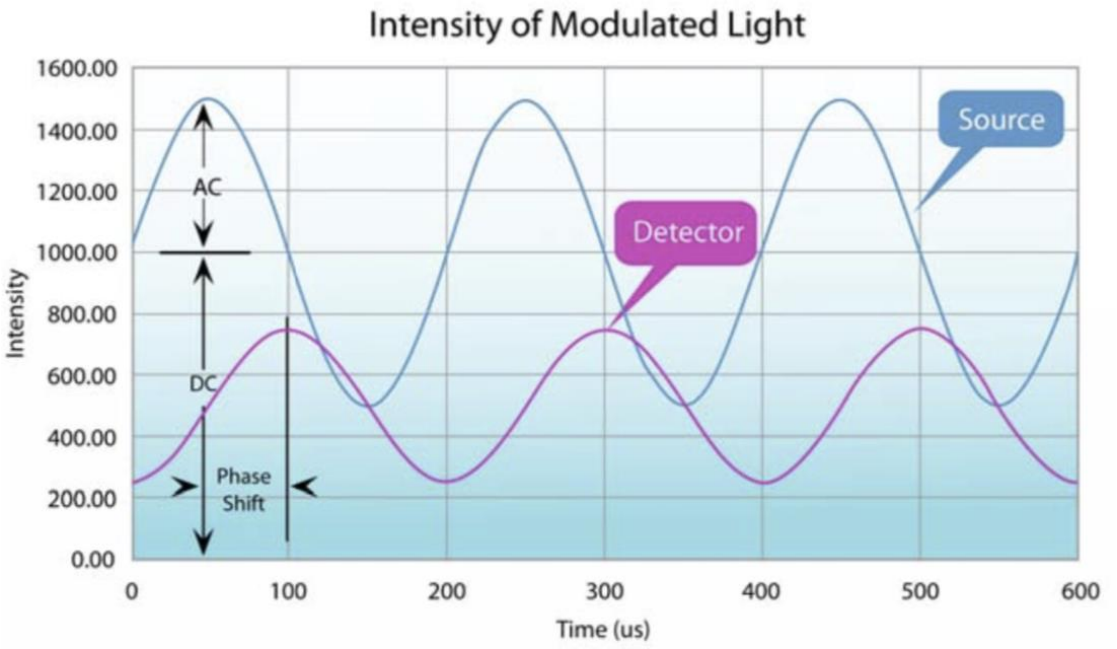

FIGURE 8: Light is modulated at 110 MHz in the FD technique used by the Imagent system to allow for determining absorption and scattering parameters. The phase shift from the delay in light emitted to light received provides the information necessary for this determination.

The amount by which these components and phase change as a function of source-detector separation allows for μ_a and μ_s' to be determined. The experimental data in the output includes values of the DC, AC, and phase components of the signal. It is exported as an ASCII file and imported to MATLAB 2018b where a custom code is used to process the data.

2.4. Signal Processing

The custom-written MATLAB 2018b program processes the signal obtained through the following sequence:

Intensity to Concentration Changes

Intensity from DC Signal [4]:

$$I_{\lambda_i R_i} = I_{DC} DCCF_i$$

Change in optical density [5]:

$$\Delta OD_{\lambda_i R_i} = log\left({}^{I_o}/_{I}\right) = \varepsilon_{Hb\lambda_1} DPF_{\lambda_1} R_i + \varepsilon_{HbO\lambda_1} DPF_{\lambda_1} R_i$$

Matrix to solve for concentration changes [6]:

$$\begin{bmatrix} \Delta OD_{\lambda_1 R_i} \\ \Delta OD_{\lambda_2 R_i} \end{bmatrix} = \begin{bmatrix} \varepsilon_{Hb\lambda_1} DPF_{\lambda_1} R_i & \varepsilon_{HbO\lambda_1} DPF_{\lambda_1} R_i \\ \varepsilon_{Hb\lambda_2} DPF_{\lambda_2} R_i & \varepsilon_{HbO\lambda_2} DPF_{\lambda_2} R_i \end{bmatrix} \begin{bmatrix} [\Delta Hb] \\ [\Delta HbO] \end{bmatrix}$$

Total Hemoglobin Concentration [7]:

$$[\Delta THC] = [\Delta Hb] + [\Delta HbO]$$

Normalizing each signal [8]:

$$Z_{Chr} = \frac{[Chr] - \bar{x}_{Chr}}{\sigma_{Chr}}$$

where,

$$[Chr] = [\Delta Hb] or [\Delta HbO] or [\Delta THC]$$

Concentration Changes to LFOs

Average FFT of 8 segments [9]:

$$F_{Chr} = \frac{1}{8}\sum FFT(Chr)$$

$$Chr^i = \begin{matrix} [\Delta HbO]^{HUT} & [\Delta HbO]^{Rest} \\ [\Delta Hb]^{HUT} & [\Delta Hb]^{Rest} \\ [\Delta THC]^{HUT} & [\Delta THC]^{Rest} \end{matrix}$$

Power spectrum density [10]:

$$PSD(f) = {}^{F^*(f) \times F(f)}/_{f_s}$$

Statistical Discovery.™ From SAS.

Ready for Analysis

The ASCII file from the OxiplexTS is imported to MATLAB 2018b as a table and transformed into a matrix. The time-series component of the output is formatted into 8 columns of direct current (DC) intensities and 8 columns of alternating current (AC) intensities. There are 8 columns of each because the combination of two wavelengths and four source-detector (Ri) separations results in eight paths of light passing through the cortex. We isolated the DC columns and adjusted these intensity values to each subject's absorption & scattering properties **(Equation 4).** The DC correlation factor (DCCF) adjusted the intensities to how well the system was estimating these properties and can be seen in Equation 4 above. We then calculated changes in optical density (OD) for each wavelength and Ri combination from intensity changes between initial light and outputted light using **Equation 5** as shown above. These OD changes can be related to the concentrations of hemoglobins, the differential path-length factor (DPF) specific to each wavelength, and each Ri as is also shown in **Equation 5**. The MBLL (**Equation 6**) was then used to determine concentration changes for each chromophore using matrix algebra. The result was four arrays of concentration changes for HbO and Hb from which THC was calculated using **Equation 7**. The Z-score , shown in **Equation 8,** was then used to center and normalize these concentration parameters as was done in a previous study[144]. The average of the four channels of each chromophore were used to obtain a single array for each normalized concentration parameter that increased signal-to-noise ratio (SNR).

For extracting LFO intensities from normalized concentration changes, Welch's method was used to obtain its power spectral densities (PSDs), as was done in previous studies[30, 31, 124]. Before beginning segmentation, the normalized arrays were filtered into specific time segments of the HUT and Rest positions to avoid capturing the transition period and focus the analysis on the two elevations. Chr^{i} in the diagram above represents the three time-series arrays analyzed by the following methods. Welch's method divided the time-series array into eight segments with 50% overlap. The frequency response of each of these segments were obtained by Fast-Fourier Transform (FFT) using the FFT command in Matlab and then they were averaged to obtain smoother spectrum (**Equation 9**). This spectrum had a frequency resolution of ~0.027 Hz, obtained by dividing the sampling frequency (fs), by the length of each segment. The LFO intensity was then obtained using **Equation 10** where Fx*(f) was the complex conjugate of Fx(f) and f was in the low frequency range of 0.05 to 0.15 Hz. The result was a PSD in units of (μM^2/Hz) for each trial. The final analysis was then performed on JMP Pro 15 and Microsoft Excel.

3. Results and Discussion

3.1. Hemodynamic Concentration Changes

While this project focuses on the frequency analysis of the fNIRS time-response signal, we first assessed the time-response of the concentration changes affected by lowering the HOB from the HUT position to the resting position. To do this, we calculated the difference in concentrations at each elevation processed through the written program in MATLAB 2018b explained previously. The **Equations [11-13]** below show the resulting parameters used for the hemodynamic concentration change analysis for each chromophore.

$$\Delta HBO(t)=[\Delta HBO_{HUT}](t)-[\Delta HBO_{Sup}](t) \quad [11]$$

$$\Delta HB(t)=[\Delta HB_{HUT}](t)-[\Delta HB_{Sup}](t) \quad [12]$$

$$\Delta THC(t)=[\Delta THC_{HUT}](t)-[\Delta THC_{Sup}](t) \quad [13]$$

3.2.1 Oxygenated Hemoglobin Changes from HOB Lowering

The individual and group mean concentration changes of HbO are shown in **Figure 9** below. The change in an individual chromophore concentration is depicted as an absolute value and trials 3, 7, and TBI_1 in **Figure 9a** represent a decrease in HbO concentration when the HOB was lowered rather than an increase. The change in mean chromophore concentration takes these decreases into account.

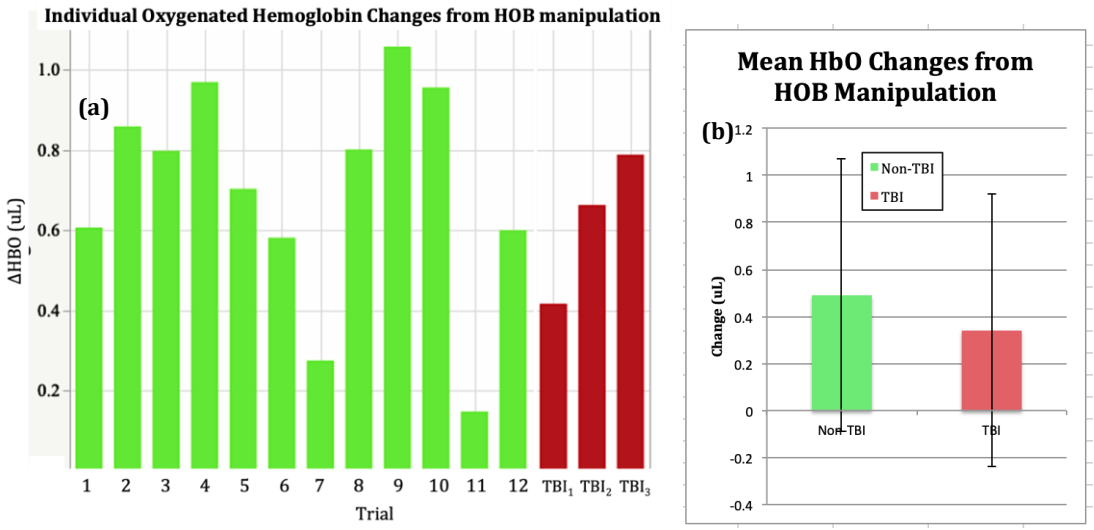

FIGURE 9: (a) Individual and (b) group mean changes in oxygenated hemoglobin as they went from HUT to resting positions. The non-TBI trials are depicted in green and the TBI trials are depicted in red.

Overall, both groups had HbO increase as the bed lowered from HUT to the resting position despite both experiencing individual trials with decreases in HbO. The non-TBI trials had greater concentration changes with the HOB manipulation with a difference of 0.15 μM. These results are consistent with previous studies where an elevated position shows lower HbO concentrations than a resting position.

3.2.2 Deoxygenated Hemoglobin Changes from HOB Lowering

Figure 10 below shows the individual and group mean concentration changes of Hb. In **Figure 10a,** trials 5, 6, 10, 11, 12, TBI 1 and TBI 3 represent a decrease in concentration when the HOB was lowered.

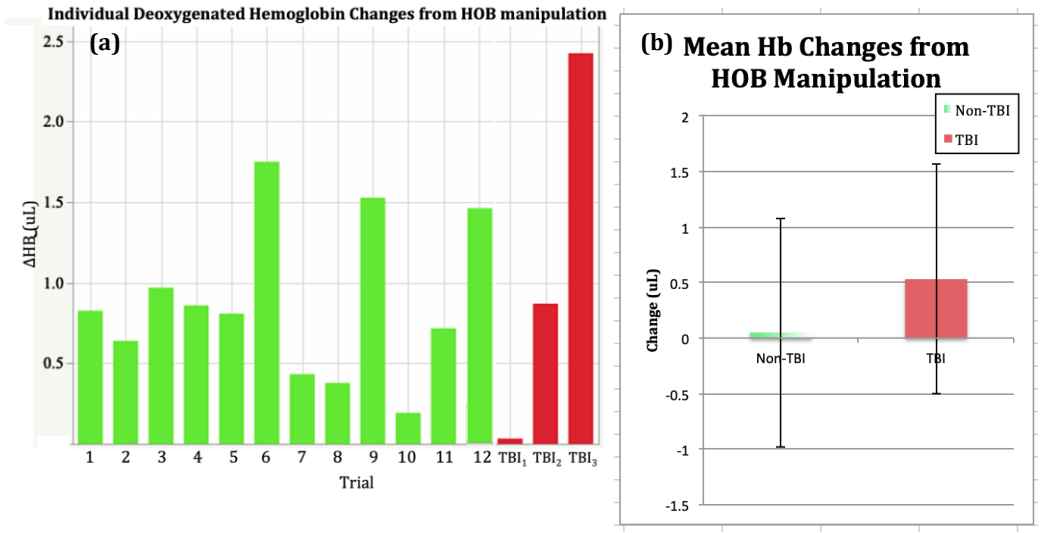

FIGURE 10: (a) Individual and (b) group mean changes in deoxygenated hemoglobin as they went from HUT to resting positions. The non-TBI trials are depicted in green and the TBI trials are depicted in red.

Overall, Hb increased in the TBI trials when going from HUT to resting. Non-TBI, on the other hand, saw an overall—albeit small, decrease in Hb concentration when lowered to the resting position. With the difference of 0.58 μM, there are distinct effects between groups regarding deoxygenated blood. The non-TBI trials are consistent with previous studies where Hb concentration decreases at the resting position. The mean effect of Hb concentration increasing in TBI, and even more significantly than its HbO increase, suggests a potential issue with regulating blood flow in injured brains.

3.2.3 Total Hemoglobin Changes from HOB Lowering

Figure 11 below shows the individual and group mean concentration changes of the total hemoglobin response. As with changes in the HbO signal, trials 3, 7, and TBI1 in **Figure 11a** represent a decrease in concentration when the HOB was lowered.

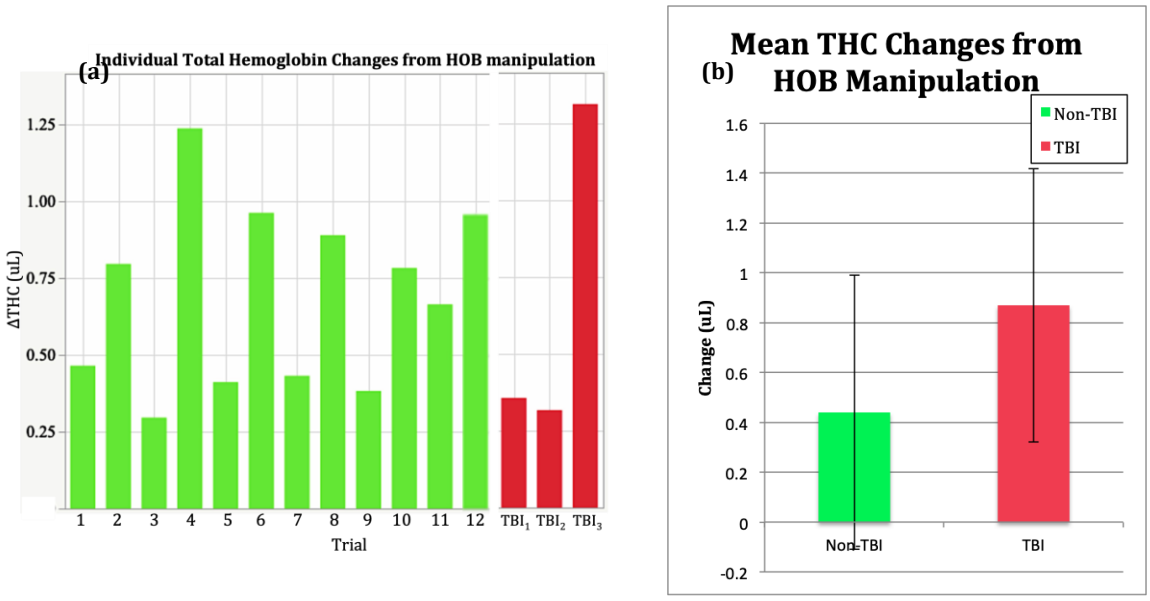

FIGURE 11: (a) Individual and (b) group mean changes in total hemoglobin as they went from HUT to resting positions. The non-TBI trials are depicted in green and the TBI trials are depicted in red.

Overall, both groups had a total increase in hemoglobin concentration as the bed lowered from HUT to the resting position. A large increase of HbO in the non-TBI trials and both HbO and Hb increasing with HOB lowering contributed to more blood present at the resting position. Comparing between non-TBI and TBI, the magnitude of changes of HbO and THC was more pronounced in TBI subjects with Hb substantially changing in the TBI trials. This latter effect of Hb is inconsistent with a previous study where HbO was the main influencer on THC. That specific study, however, assessed healthy populations whereas this discrepancy occurs in a brain-diseased population. This further strengthens the idea that injured brains regulate blood flow differently than healthy ones. Figure 12 below summarizes the hemodynamic concentration changes discussed in this section.

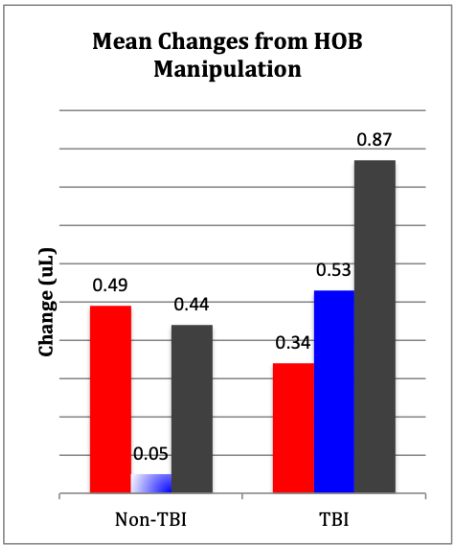

FIGURE 12: Summary of group mean changes in oxygenated (red), deoxygenated (blue), and total hemoglobin (black) as they went from HUT to resting positions.

3.3. Changes in Low Frequency Oscillations

Initially, viewing the data from a frequency analysis yielded ambiguous results. To assess the changes in frequency response of a subject from HUT to the resting position, we generated an average low frequency spectrum during the two respective elevations were generated.

We excluded the data during the time the bed was actively being lowered from 30° to 0° to exclude transition effects and isolate the positions of interest. A representative time-series data is shown in **Figure 13**, where the HUT and Rest time-segments are labelled, which indicates the time periods isolated to represent HUT and resting positions. Future studies could look at these transition periods to investigate whether frequency or time domain information during the transition could characterize trauma in the brain, however this was beyond the scope of this project.

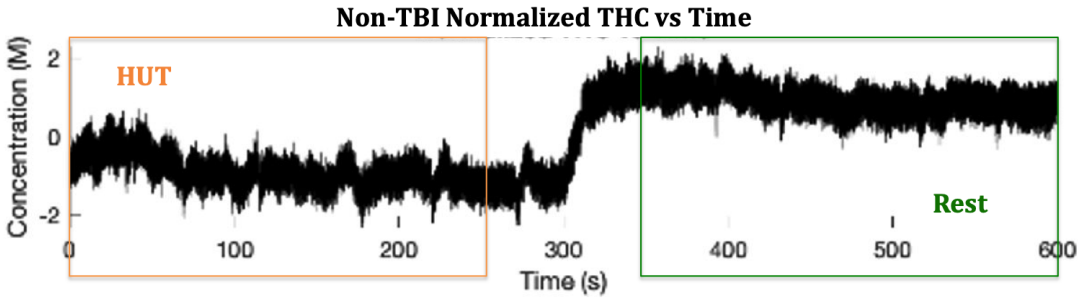

FIGURE 13: Example time series of a non-TBI trial showcasing the time-series filtering of the signal to separate HUT and Rest to be representative of the elevations only and exclude the transition effects.

To characterize TBI and the impact of changing a subject's elevation we divided our observations into two comparisons: 1) between study groups at each elevation, and 2) between elevations within each study group.

3.3.1 HUT comparison between study groups at each elevation

These frequency responses are shown in Figure 14 below. The responses include a non-TBI plot during HUT (Fig.14a), a non-TBI plot during the resting position (Fig.14b), a TBI plot during HUT (Fig.14c), and a TBI plot during the resting position (Fig.14d).

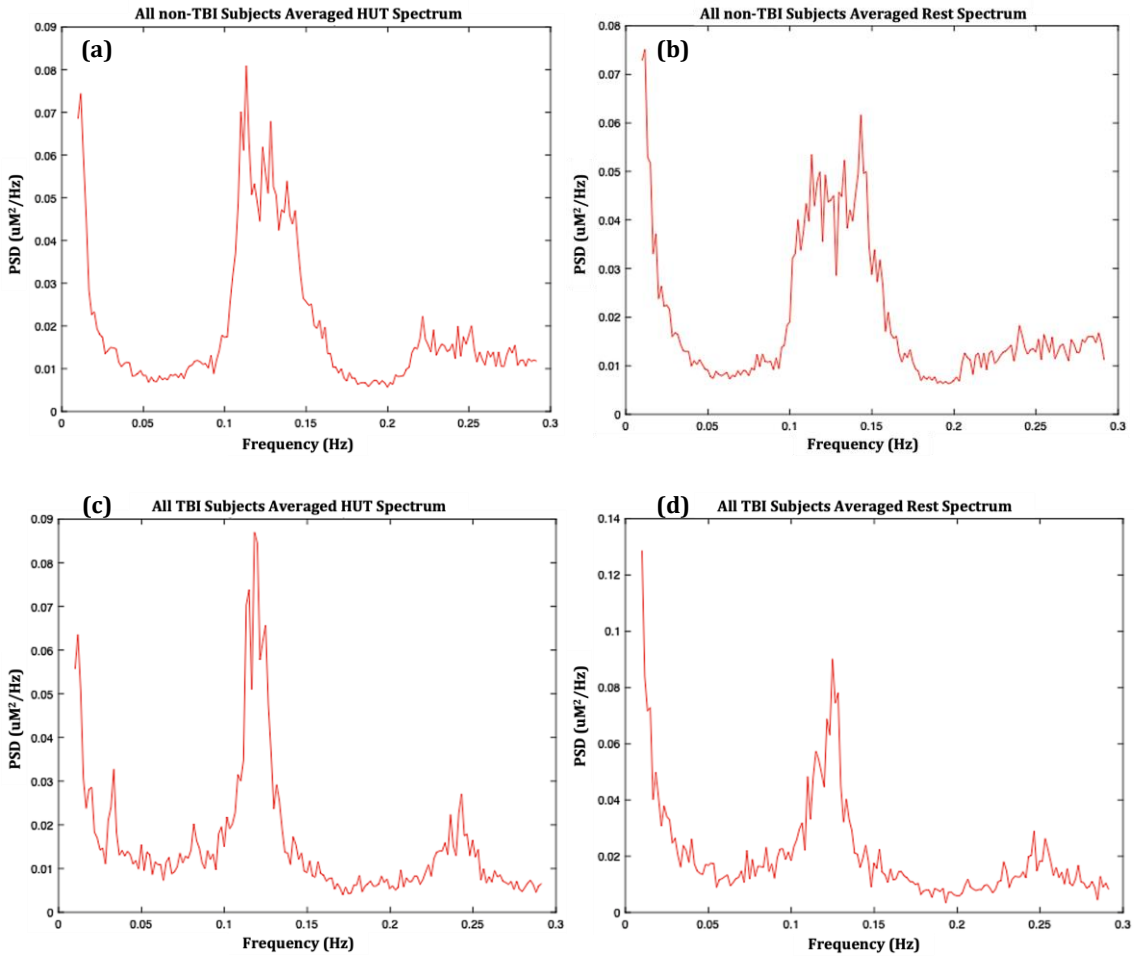

FIGURE 14: Frequency spectrums of the average of all HbO trials within each group: (a) the non-TBI spectrum during HUT, (b) the non-TBI spectrum at the resting position, (c) the TBI spectrum during HUT, and (d) the TBI spectrum at the resting position.

Comparing between **Figure 14a** and **Figure 14c**, the frequency response between non-TBI and TBI at the elevated (HUT) position is generally similar in shape. Both groups show significant activity within the [0.1-0.15] Hz range and a smaller, yet notable response beginning at ~0.2 Hz. The significant activity around 0.1 Hz is consistent with previous studies of spontaneous LFOs where they were observed in MAP and CBFV signals[30]. Interestingly, their PSD is similar between the two groups at this HUT position, with max intensities of ~0.08 $\mu M^2/Hz$. This suggests and strengthens the findings of previous studies of an intrinsic neuronal mechanism occurring at this 0.1 Hz oscillation and could be a

frequency of choice when comparing between healthy and diseased states. With this thesis showing a similar PSD distribution in this elevated HUT position at 0.1 Hz, this could allude to the cerebral response favoring and regulating at a normal level in the HUT position, regardless of it is injured or healthy. **Figure 14c**, however, provides insight on a frequency that could differentiate TBI in the HUT position. There is a significant increased response at ~0.027 Hz in the TBI group at HUT that is not observed in the non-TBI group at HUT. This is consistent with a study comparing children with autism spectrum disorder (ASD) and typically developing (TD) children where they observed stronger fluctuation magnitude in the 0.0200-0.0333 Hz band in ASD trials that did not exist in their TD trials. In that study, subjects were also at an elevated position as they were asked to sit upright in a chair with their eyes closed during measurements. In our project, this stronger fluctuation is not present in the TBI trials at the resting position suggesting that the ~0.027 Hz frequency could be associated with a mechanism in the injured brain trying to autoregulate at an elevated position. Since this project had limited TBI subjects to sample, this presents an opportunity for future studies to focus on this frequency band in injured individuals specifically at an elevated position.

Regarding the spectrum distribution, the TBI trials show a narrower response than the non-TBI trials, but this is most likely due to the higher variability present in the non-TBI group from including more subjects. This is more easily seen when looking at each individual trial in **Figures 15a** and **15c** where the individual LFO spectrums from each trial of the two study groups at both elevations are shown.

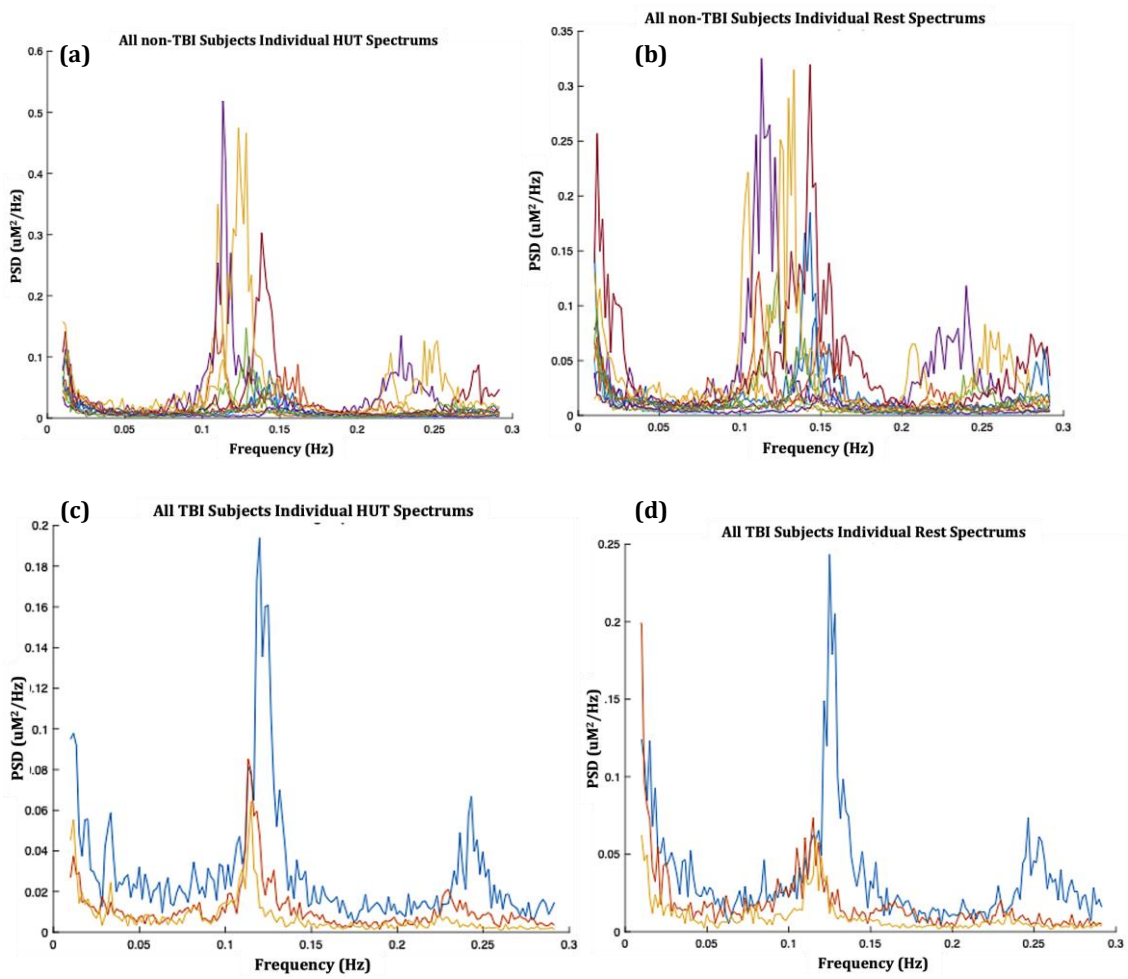

FIGURE 15: Frequency spectrums of individual HbO trials within each group: (a) the non-TBI spectrum during HUT, (b) the non-TBI spectrum at the resting position, (c) the TBI spectrum during HUT, and (d) the TBI spectrum at the resting position.

Within the 0.1-0.15 Hz band where stronger fluctuations existed in the averaged response, one can see stronger fluctuations in narrower frequencies specific to each individual subject. One non-TBI subject, for example had a notable response closer to ~0.11 Hz while another saw this stronger magnitude closer to ~0.14 Hz. Regarding the increased average response beginning around ~0.2 Hz, it is clear that this was largely influenced by one specific non-TBI subject seeing a notable increase in magnitude around ~0.225 Hz where another non-TBI subject saw this closer to ~0.25 Hz. This latter healthy response is more consistent with the TBI subject who also saw stronger magnitude closer to ~0.25 Hz

suggesting that this oscillation range beginning at ~0.2 Hz is intrinsic to CA mechanisms and was not affected in this specific TBI subject.

These results suggest that the LFO metric could also be an individualized tool to compare a subject's normal functioning frequency response to their diseased response rather than a group average comparison between injured and non-TBI populations. While this requires a closer look at intrasubject variability, **Figure 15c** indicates similar frequency responses between the TBI subject's three trials during HUT. This subject consistently had stronger magnitude fluctuations around ~0.12 Hz. These repeatable LFO responses present a high potential for individualized diagnostic measures for the brain using a practical and low-cost tool in fNIRS. However, studies with higher sample sizes should investigate this further as repeated measurements were only taken for the single TBI subject whereas the non-TBI subjects received only one measurement each.

While there is high potential with studying intersubject variability and individual diagnosis, the averaged response of larger populations such as TBI and non-TBI should not be ignored as certain frequency bands of interest can be identified. The consistently increased spontaneous activity around frequency bands of 0.1-0.15 Hz and ~0.2 Hz between all averaged TBI and non-TBI trials suggests these frequencies may be of high interest for CA assessment at elevated positions.

3.3.2 Rest comparison between study groups at each elevation

Comparing between **Figure 14b** and **Figure 14d**, the non-TBI trials exhibit significant activity in the 0.1-0.17 Hz range in the resting position while the TBI trials also see activity, but from the 0.1-0.14 Hz range. There is also a rise in fluctuation beginning at the ~0.2 Hz

in the non-TBI group while this increase in activity begins at ~0.225 Hz for the TBI trials. This is inconsistent with the previous study mentioned where the only significant frequency response was from the HUT position and the flat resting (Rest) position did not show peaks near ~0.1 Hz. A difference in protocol could explain this discrepancy. In that study, subjects were first measured in the flat resting position and then transitioned to the HUT position. In this project, on the other hand, subjects were initially measured in the HUT position and then lowered to the flat resting position. The frequency activity present in this project could therefore still be indicative of a lingering cerebral mechanism from an elevated posture and future studies should consider measuring the flat resting position prior to the HUT position. The presence of ~0.1 Hz frequency activity in both the non-TBI and TBI trials at this resting position shows that trauma to the brain in this subject did not affect the underlying mechanism that this 0.1 Hz oscillation represents. In fact, the PSD is stronger in magnitude in the TBI trials compared to the non-TBI trials, however more TBI subjects are necessary to ensure it is representative of the TBI population and not unique to this subject.

Similarly to the HUT discussion, **Figure 14b** and **Figure 14d** related to the resting position also shows the limitations of drawing conclusions based on group averages characteristic of the TBI population. This is evident from the frequency response of individual non-TBI subjects in **Figure 15b**. A few of these non-TBI trials exhibit stronger magnitude near the same ~0.11 Hz frequency as the TBI trials. Others exhibit a similar response again between non-TBI and TBI near the ~0.25 Hz frequency and suggest LFO analysis to characterize TBI should be considered on a case-by-case basis.

3.3.3 Non-TBI comparison between elevations within each study group

Comparing between **Figure 14a** and **14b**, the non-TBI subjects show a wider LFO range at rest than at HUT. The lower variability in the HUT position of the same subjects could suggest two things: 1) it conveys higher precision power in measuring subjects at an elevated position, and/or 2) there is recruitment of more underlying mechanisms for CA that are represented by more frequencies at the flat resting position than at an elevated position. The first theory is supported by the previously mentioned study by Cheng et al.[30]. In the frequency response from the flat resting position, their healthy subjects had low success rates for identifying LFOs with large frequency ranges (0.078-0.086 Hz) and standard deviations. Conversely in the HUT position, their subjects exhibited 100% success rates for identifying LFOs and a focused ~0.076 Hz response with smaller standard deviations. Regarding PSD magnitude, the HUT position shows a higher overall magnitude for the non-TBI trials compared to the resting position for the same trials. A predominant difference between HUT and resting position is observed at around 0.115 Hz. This frequency is notable in the HUT position but significantly lowers in the resting position. Conversely, a peak in the frequency ~0.14 Hz in the resting position does not exist in the HUT position.

From **Figures 15a** and **15b**, it is evident that this differentiation between HUT response and flat resting response results from individual subjects rather than a group average. The peak at ~0.14 Hz results from only two subjects exhibiting a significant response in this region, while most subjects did not contribute to the peak. Additionally, the widened response that includes more frequencies in the resting position than in the HUT position is

the result of two different individuals. In **Figure 15b**, one can see the subject represented by the yellow spectrum is responsible for the widening of the averaged response as it showed a peak near ~0.1 Hz that was not present in the HUT position. The subject represented by the red spectrum is responsible for the widening of the averaged response on the other side of the range as it shows a peak near ~0.17 Hz that was not present in the HUT position. Therefore, the widening was not the result of a single subject going from HUT to rest, but rather a larger variation in a few subjects. These individual responses support the second theory that there could be underlying mechanisms for CA expressed in these two individuals that are not recruited at an elevated position. However, since they are only present in two trials it would require further investigation and favors the idea that LFO responses are unique to each subject's normal functioning. On another hand, a higher overall power in the HUT responses shows the strength of using this elevated head position as a reliable protocol for assessing LFO responses.

3.3.4 TBI comparison between elevations within each study group

Comparing between **Figure 14c** and **Figure 14d**, the frequency response does not seem to change much from HUT to rest in the TBI trials, especially around the 0.1-0.14 Hz range. The strongest PSD magnitude in both positions around ~0.12 Hz is also consistent in power between the two positions. When looking at the activity beginning near ~0.2 Hz, fluctuations are present in both positions, as was seen in the non-TBI trials. However, the overall power is higher in the resting position compared to the HUT position here whereas in the non-TBI trials the power in this frequency region remained fairly similar and even showed an overall decrease at the resting position. The most prominent difference,

however, between the HUT and resting position in these TBI trials is the peak seen in the HUT position at ~0.027 Hz that is negligible in the resting position. This peak is also not present in either position in the non-TBI trials. As was previously mentioned, this observation correlates with responses seen in the study on ASD children measured at an elevated position. The ~0.027 Hz frequency, therefore becomes an identifiable feature of diseased brain states and should be followed up in subsequent studies.

Regarding the individual TBI trials in **Figures 15c** and **15d**, the LFO responses remain consistent when going from HUT to rest. The main difference is a higher power in one of the trials in the ~0.12 Hz peak that was countered by a lower power in the other two trials which resulted in a consistent averaged response. The lack of change in the LFOs when going from HUT to resting in these TBI trials differs from the individual non-TBI changes when going from HUT to rest. In those non-TBI trials, subjects either showed increased or decreased magnitudes in their PSD at these observed frequencies. This suggests that the injured brain did not respond adequately to a change in elevation whereas non-injured brains usually adjust their underlying mechanisms when undergoing elevation changes. This is another hypothesis that should be considered in future studies with larger sample sizes and shows the strength of using HOB manipulation to characterize TBI. The repeatability of responses in the three trials from this TBI subject, however, show the strength of fNIRS to identify meaningful LFOs in studying trauma in the brain. Therefore, in future studies with larger sample sizes, fNIRS and LFO analysis remains a suitable metric for characterizing TBI.

3.3.5 Defining frequencies of interest through prevalence analysis

To further identify frequencies of interest to guide future LFO analysis in the TBI population, the prevalence of increased activity of certain frequencies was analyzed. To do this, peaks at specific frequencies from the spectrum of each subject were identified using the program built in MATLAB 2018b and a count was kept of each frequency of interest as well as its PSD magnitude value. A frequency was considered a peak if its PSD magnitude was greater than the value of its neighbouring observations. An example of an individual subject's peak data collection is included in **Figure 25** in the Appendix. The peak frequencies of each trial were then compiled into one table and imported into JMP Pro 15 for the prevalence analysis. The distribution of peak frequencies for each population at each elevation was then plotted on JMP and is visible in Figure 16 below. We limited our analysis of frequencies up to 0.1 Hz to compare to previous studies' focus on these LFOs. However, previous studies did not look at prevalence as a metric. It serves more of an observational premise to guide future studies to LFOs of interest.

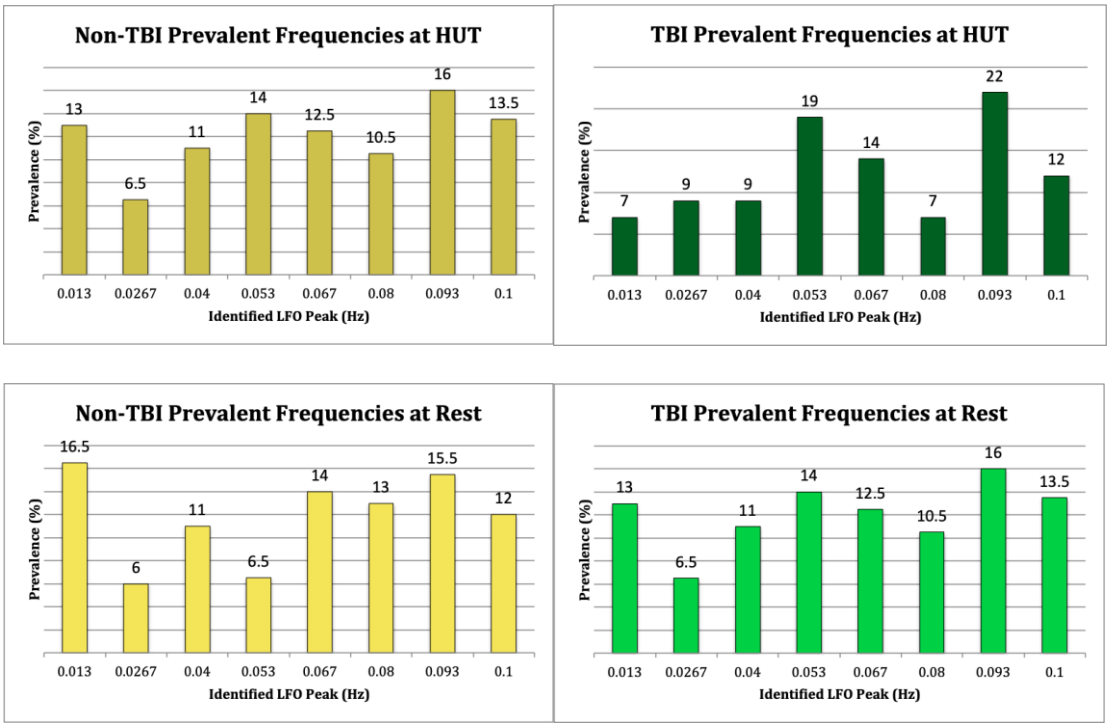

FIGURE 16: JMP distribution of peak frequencies for each population at each elevation.

Peaks near ~0.013 Hz were prominent in non-TBI trials with a similar slightly higher prevalence in the resting position. In TBI trials, this frequency was significantly more pronounced in the resting position. The 0.04 Hz LFO also was present in numerous spectrums, consistently in the non-TBI group and more prevalent at the resting position in the TBI group. Peaks near ~0.053 Hz also warrant attention as they are prominent in the HUT position in both non-TBI and TBI trials and drop in prevalence when going to the resting position. The ~0.067 Hz peak is also notable in non-TBI and TBI trials, remaining fairly consistent among elevations. The ~0.08 Hz peak slightly increased in prevalence when comparing HUT to resting in both groups. This specific LFO is also mentioned in previous studies as a potential intrinsic property of the brain that plays an important role in brain organization[131–134]. Its smaller prevalence in the TBI trials at the HUT position conveys that ~0.08 Hz could be characteristic of an underlying mechanism that becomes

affected with trauma to the brain. The ~0.093 Hz peak emerged as the most prevalent LFO and is fairly consistent in the HUT and resting positions for the non-TBI trials, while it slightly lowers in the resting position. Like the ~0.08 Hz peak, this ~0.093 Hz peak could be a defining frequency that should be considered in future TBI studies. The ~0.1 Hz was also prevalent in both groups and remained fairly consistent in prevalence as a peak between HUT and the resting positions. These last three frequencies identified as potential LFOs of interest belong to a range of frequencies that several studies say may be linked to CA[124–126] Additionally, they belong to the slow-3 band described in the following analysis.

3.3.6 Slow Bands Analysis

As was previously mentioned, the research community has begun to define frequency ranges representative of brain functions in these lower frequency values. Termed "slow-bands", these five ranges are garnering attention in characterizing brain disease in a variety of technologies including EEG, fMRI, and fNIRS. The slow-5 band includes 0.01–0.027 Hz, the slow-4 band includes 0.027–0.073 Hz, the slow-3 band includes 0.073–0.198 Hz, the slow-2 band includes 0.198–0.25 Hz, and the slow-1 band includes 0.5-0.75 Hz. **Figure 17** below shows the individual and averaged spectrums of all trials for the non-TBI population and **Figure 18** shows them for the TBI population during the entire measurement period. This means frequencies present during the transition period are included in these spectrums.

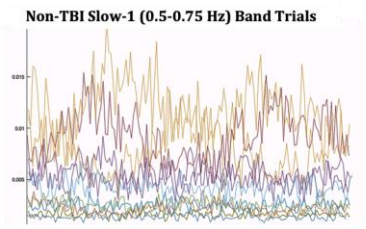
Non-TBI Slow-1 (0.5-0.75 Hz) Band Trials

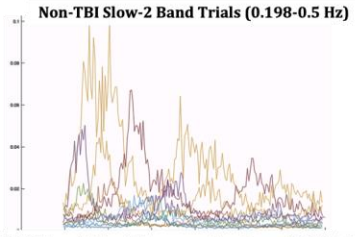
Non-TBI Slow-2 Band Trials (0.198-0.5 Hz)

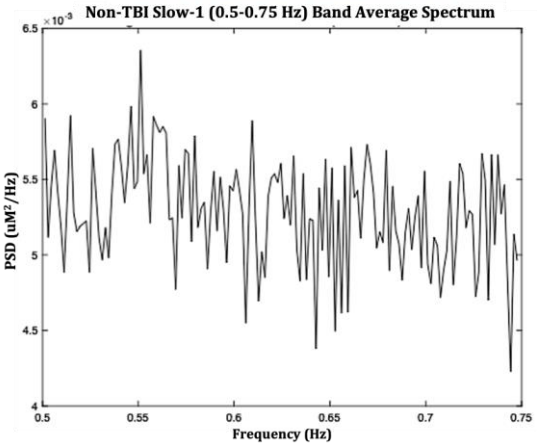
Non-TBI Slow-1 (0.5-0.75 Hz) Band Average Spectrum
PSD (uM²/Hz)
Frequency (Hz)

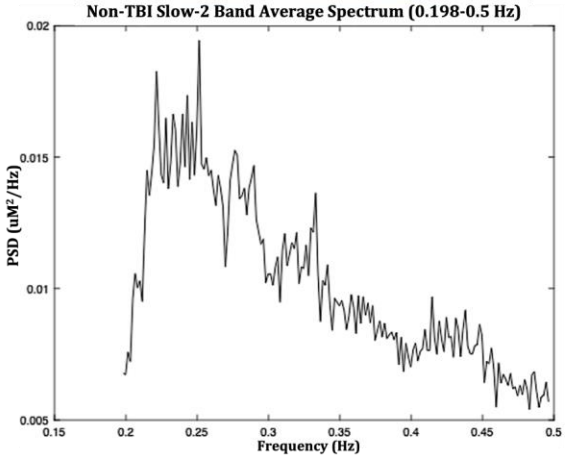
Non-TBI Slow-2 Band Average Spectrum (0.198-0.5 Hz)
PSD (uM²/Hz)
Frequency (Hz)

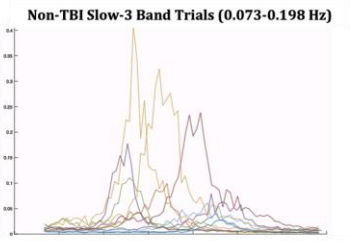
Non-TBI Slow-3 Band Trials (0.073-0.198 Hz)

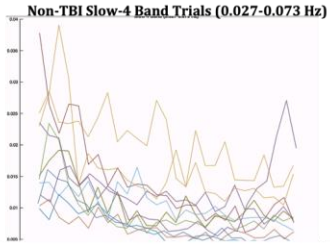
Non-TBI Slow-4 Band Trials (0.027-0.073 Hz)

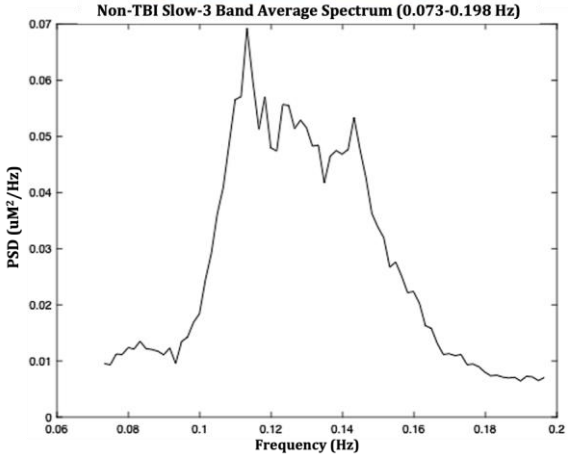
Non-TBI Slow-3 Band Average Spectrum (0.073-0.198 Hz)
PSD (uM²/Hz)
Frequency (Hz)

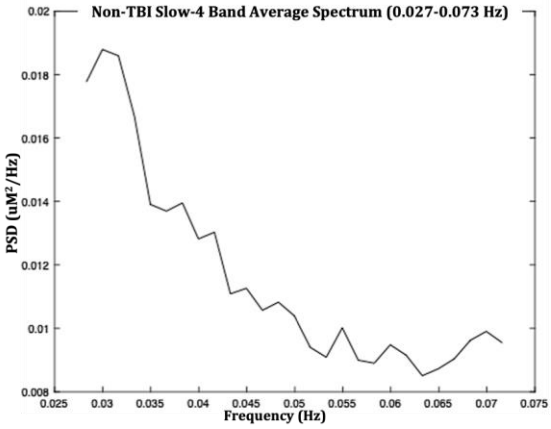
Non-TBI Slow-4 Band Average Spectrum (0.027-0.073 Hz)
PSD (uM²/Hz)
Frequency (Hz)

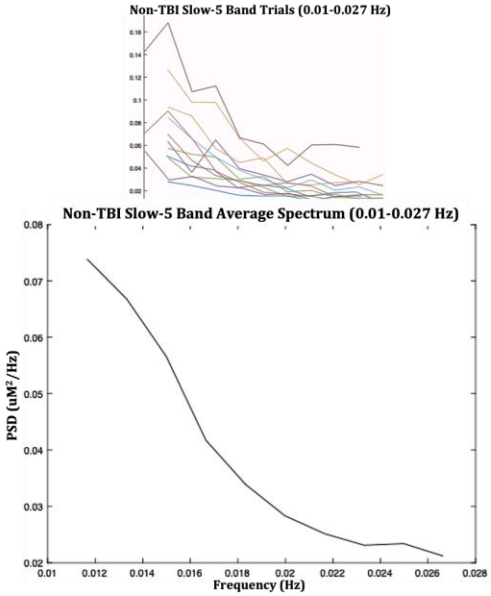

FIGURE 17: The individual trials and averaged spectrums of each slow band for the non-TBI population.

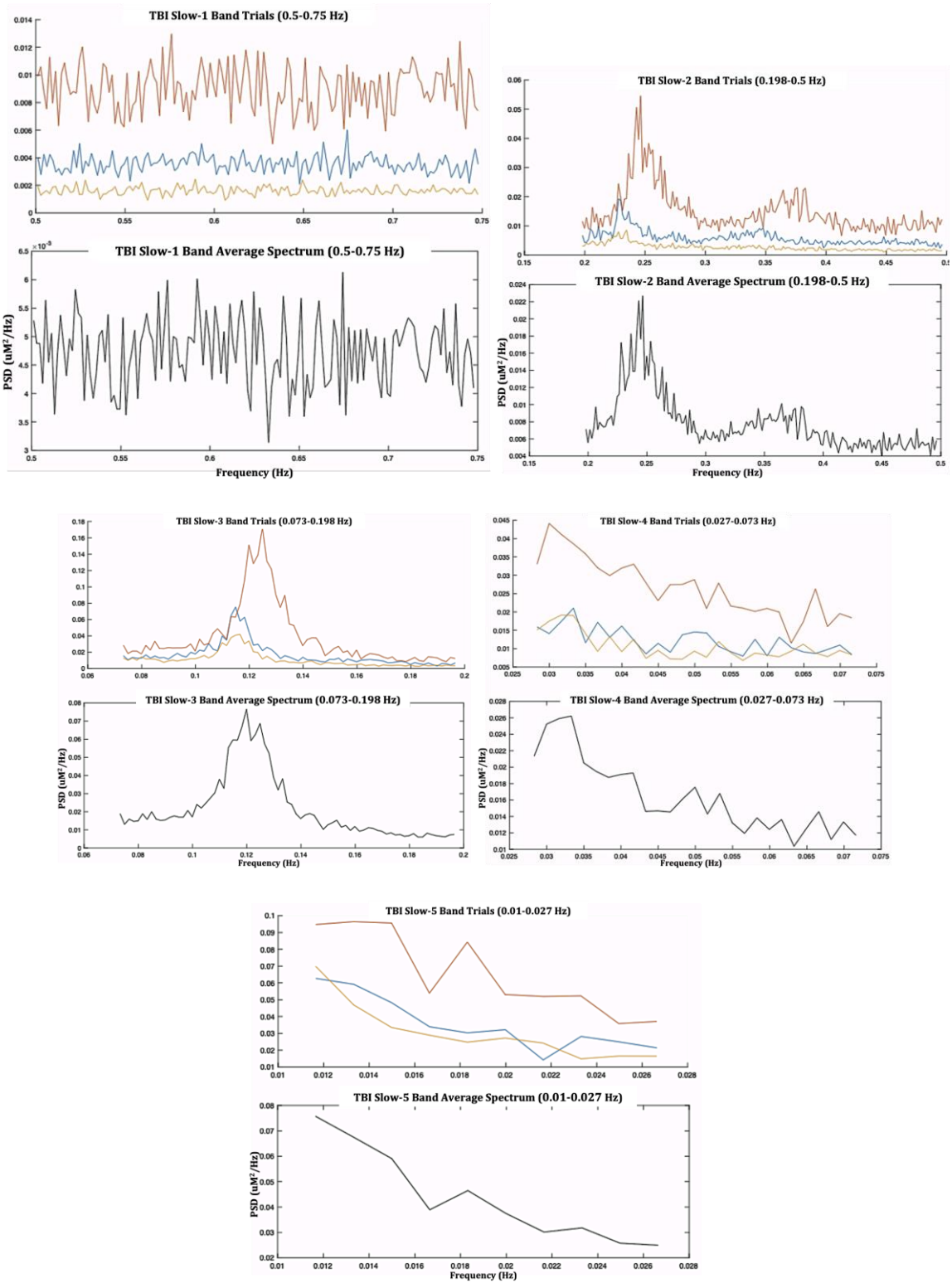

FIGURE 18: The individual trials and averaged spectrums of each slow band for the TBI population.

Two approaches used to provide quantitative metrics from these bands included: 1) averaging the power spectrum of each band and 2) isolating the maximum PSD magnitude within each band. The latter was chosen as a method of interest from the presence of discrete peaks in the spectrums that are especially observable in the slow-2 and slow-3 bands. Maximum values within each band, therefore, characterize the more prevalent frequencies and could provide valuable information that an averaged value might conceal. This is most important when assessing the slow-3 band where most subjects saw pronounced activity near the 0.1 Hz frequency rather than representing the entire 0.078-0.198 Hz range. Therefore, the overall average value obtained from the slow-3 band for each population largely differs from the average maximum power in this band.

3.3.7 Slow Band Average Power Analysis

For the first analysis, the average PSD magnitude of each slow band was obtained from each trial using the program created in MATLAB 2018b. We separated each trial's average PSD within each slow band at both HOB positions (HUT and Rest) using the time-series filtering previously described. **Figure 26** in the Appendix shows an example of the individual spectrums of one subject at the two HOB positions. The average PSDs in units of uM^2/Hz for each trial were recorded in **Table 3** found in the Appendix. Percent change was then used to assess the effects of HOB manipulation and observe if differences existed between the non-TBI and TBI trials at the two elevations. Percent change is defined in **Equation 14** below and this data is included in **Table 4** in the Appendix.

$$\% \text{ Change} = 100 \times (PSD_{HUT} - PSD_{REST}) / PSD_{REST} \quad [14]$$

From the percent change data, we assessed changes by determining the prevalence of average power increases (APIs) and decreases (APDs) when comparing the HUT position to the Rest position. An API was defined as a positive percent change from a higher power present at HUT, and an APD was defined a negative percent change and a lower power present at HUT. In the non-TBI population, APIs were more prevalent at the HUT position for the slow-3 and slow-5 bands, APDs were more prevalent for the slow-1 band, and the prevalence was equal of APIs and APDs for the slow-2 and slow-4 bands. In the TBI population on the other hand, all trials saw APDs at the HUT position for all five slow bands. A summary of these observations is shown in **Figure 19** below.

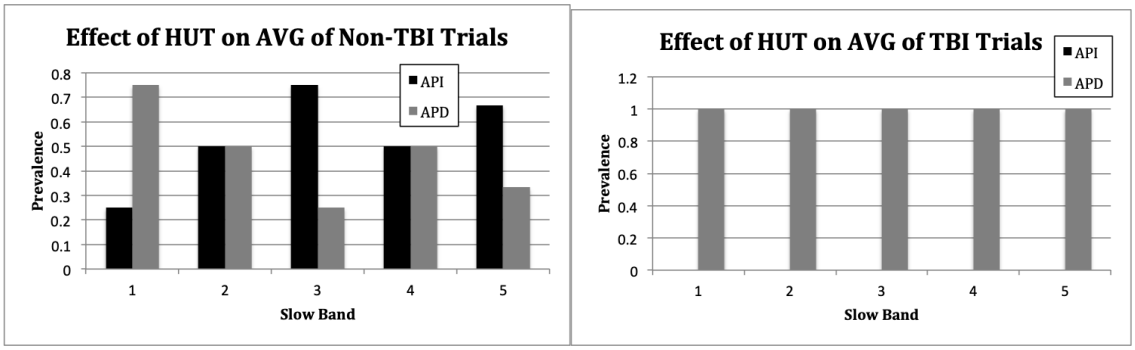

FIGURE 19: The prevalence of average power increases (APIs) and decreases (APDs) from the subjects at the HUT position in comparison to their resting position power. (Left) Compares APIs and APDs in the non-TBI trials and (right) compares them in the TBI trials.

To take the magnitude of the percent changes into consideration, we averaged the percent changes of the trials within each population and slow band to determine the overall population effects of the HUT position. These results are summarized in Figure 19 below. In the slow-1 band of the non-TBI trials, we observed an overall 33.5% increase in power with HUT, despite there being more prevalence of APDs for this band. Two subjects with a 363% and 122% increase respectively largely influenced the overall average increase and show the strength of assessing change on an individual basis. In the slow-1 band of the TBI trials, we observed an overall 5.3% decrease in power with HUT consistent with the

prevalence of decreases within those trials. Looking at **Figure 20**, it is evident that individual trials within the non-TBI group exhibited similar LFO effects to the TBI trials suggesting that the effects of HOB manipulation are more representative of individual brain variability rather than brain injury effects. In the slow-2 band of the non-TBI trials, we observed an overall 0.9% decrease in power with HUT consistent with an equal presence of APIs and APDs for these trials. In the slow-2 band of the TBI trials, we observed an overall 13.2% decrease in power with HUT consistent with the prevalence of APDs. In the slow-3 band of the non-TBI trials, we saw an overall 5.1% increase in power with HUT consistent with the higher prevalence of APIs, however this increase is smaller and not representative of some increases as large as 59%. In the non-TBI trials we saw an overall 20.2% decrease also consistent with its prevalence of APDs in that population. In the slow-4 band of the non-TBI trials, we saw an overall 4.0% decrease in power with HUT representative of the equal prevalence of APIs and APDs in that band. In the slow-4 band of the TBI trials, we observed an 18.9% decrease representative of the APDs in that band. In the slow-5 band of the non-TBI trials, we saw an overall 10.6% increase in power with HUT consistent with the prevalence of APIs. However, the percent changes varied from as high as 107.9% and as low as 7.1% suggesting once again the individuality of cerebral response to HOB manipulation. In the TBI trials, we saw an overall 38.8% decrease largely influenced by a 64.6% decrease observed in the second trial and consistent with the prevalence of APDs within that population.

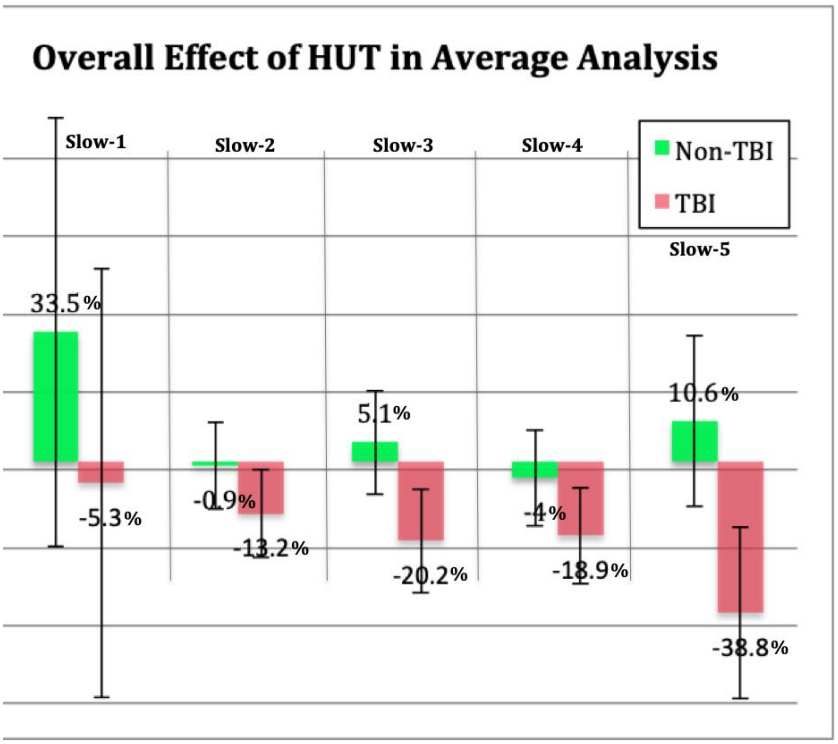

FIGURE 20: The average of percent changes comparing subjects at the HUT position to their resting position within each population and slow band.

The similarity of changes between the TBI trials, obtained from the same subject, suggest fNIRS is adequately detecting meaningful LFOs. Since there is small intrasubject variability, it suggests the LFO percent changes are representative of that subject's oscillatory mechanisms.

An average value of PSD magnitude was then obtained at each slow band to allow for comparison between the non-TBI and the TBI trials within each HOB position. Exact PSD values in uM^2/Hz are recorded in **Table 5** in the Appendix and the results are summarized in **Figure 21** below.

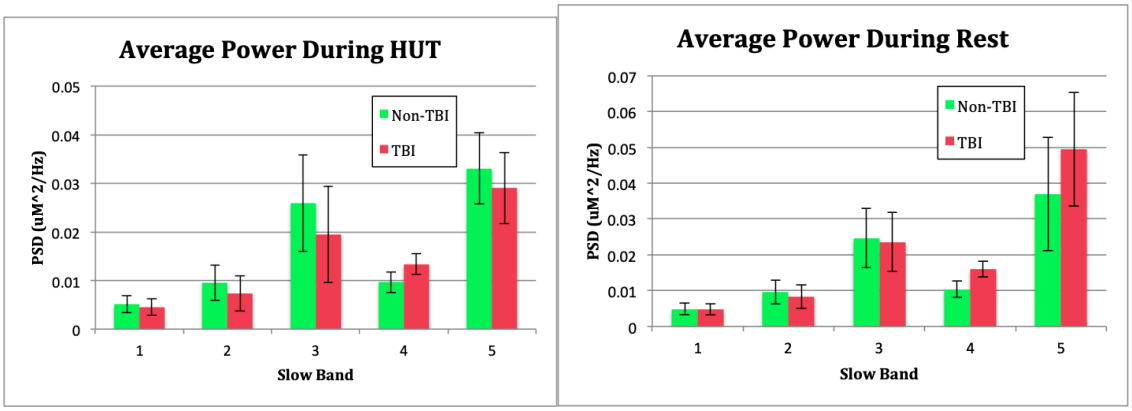

FIGURE 21: Comparison of average PSD of the non-TBI trials and TBI trials during (left) HUT and (right) the Rest position. These values can be found in Table 5 in the Appendix.

Regarding the HUT position, the non-TBI trials showed a higher power than the TBI trials in all the slow bands except for the slow-4 band. Similarly in the resting position, the non-TBI trials showed a higher power in all the slow bands except for the slow-4 and slow-5 bands. By having higher spontaneous activity of slow-1, slow-2, and slow-3 LFOs in non-TBI trials at both HOB positions, these results convey that within these three slow bands, the uninjured brain is more active than the injured brain in the mechanisms each of those bands represent. This suggests that with injury comes a decrease in activity for those three bands. Conversely, by having higher spontaneous activity of slow-4 LFOs in TBI trials at both HOB positions, these results convey that injury increases activity of the mechanism that the slow-4 band represents. This differentiation at the slow-4 band relates to a previous study that found differences from healthy controls in the slow-4 and slow-5 frequency band, however that study measured the occipital region of the brain[139].

3.3.8 Slow Band Max Power Analysis

For the second analysis, the maximum PSD magnitude of each slow band was individually isolated from each trial in MATLAB 2018b and recorded **in Table 6** in the Appendix.

Percent change was once again used to assess the effects of HOB manipulation and these changes are recorded in Table 7 in the Appendix.

In the non-TBI population, APIs were more prevalent at the HUT position for the slow-1, slow-3, and slow-4 bands, and APDs were more prevalent for the slow-2 and slow-5 bands. In the TBI population, APIs were more prevalent at the slow-2 and slow-3 bands, and APDs were more prevalent at the slow-1, slow-4, and slow-5 bands . A summary of these observations is shown in **Figure 22** below.

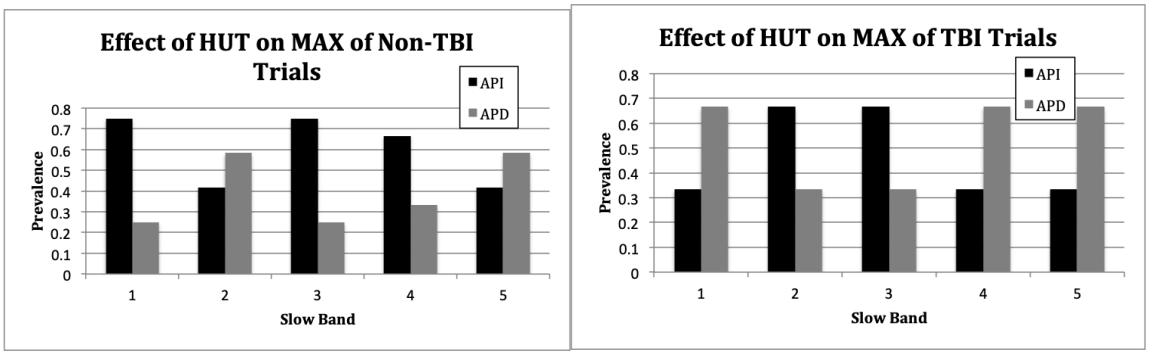

FIGURE 22: The prevalence of max power increases (APIs) and decreases (APDs) from the subject at the HUT position in comparison to their resting position power. (Left) Compares APIs and APDs in the non-TBI trials and (right) compares them in the TBI trials.

As before, we considered the magnitude of the percent changes by averaging the magnitude of the percent changes within each band of the two populations. These results are summarized in **Figure 23** below. It is important to note, however, that while the spectrums were similar amongst trials, the maximum PSD did not occur at the same frequency within each band. Therefore, an average percent change of maximum power represents more the responsiveness of LFOs within each band rather than the changes of a specific frequency. In the slow-1 band of the non-TBI trials, we observed an overall 16.2% increase in maximum power values with HUT consistent with more prevalence of APIs. In the slow-1 band of the TBI trials, we observed an overall 23.3% decrease in maximum power consistent with prevalence of APDs within those trials. In the slow-2 band of the non-TBI

trials, we observed an overall 8.5% decrease in maximum powers with HUT consistent with higher prevalence of APDs. However, one trial decreased by as much as 53.4% and as low as 2% showing large intersubject variability and the need to look at individual responses more on a case-by-case basis. In the slow-2 band of the TBI trials, we observed an overall 9.6% increase in maximum power consistent with prevalence of APIs within those trials. In the slow-3 band of the non-TBI trials, we observed an overall 13.2% increase in power values consistent with the prevalence of APIs. In the non-TBI trials, we observed an overall 0.7% increase consistent with the prevalence of small APIs within that population. In the slow-4 band of the non-TBI trials, we saw an overall 6.3% increase in maximum power consistent with the prevalence of APIs with HUT, however this small increase is not representative of trials that saw increases as large as 62.3%. In the slow-4 band of the TBI trials, we saw an overall 12.9% decrease consistent with the prevalence of APDs. In the slow-5 band of the non-TBI trials, we saw a small 2.4% overall increase in maximum power inconsistent with the larger prevalence of APDs in trials. An average increase in maximum power was most likely influenced by trials with increases as large as 68.4% and trials with decreases as small as 4.7%. Therefore, despite more non-TBI subjects experiencing a decrease in maximum power with HUT, the overall effects for that population suggests HUT minutely increases the power of maximum frequencies in the slow-5 band. In the slow-5 band of the TBI trials, we saw an overall 4.6% decrease in maximum power consistent with the higher prevalence of small APDs.

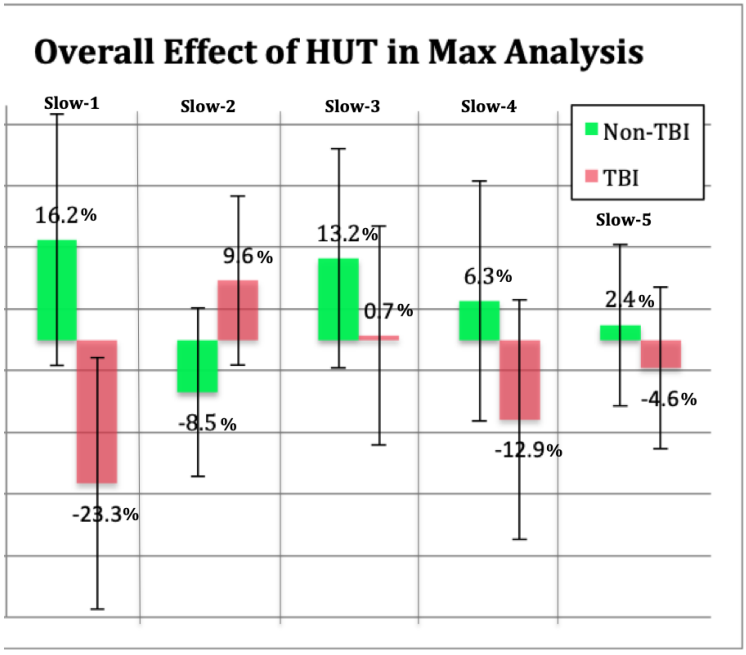

FIGURE 23: The average of max percent changes comparing subjects at the HUT position to their resting position within each population and slow band.

As with the average value analysis, the average of *maximum* PSD magnitudes was also obtained at each slow band to allow for comparison of responsiveness between the non-TBI and the TBI trials within each HOB position. Exact PSD values in uM^2/Hz are recorded in Table 8 in the Appendix and the results are summarized in **Figure 24** below.

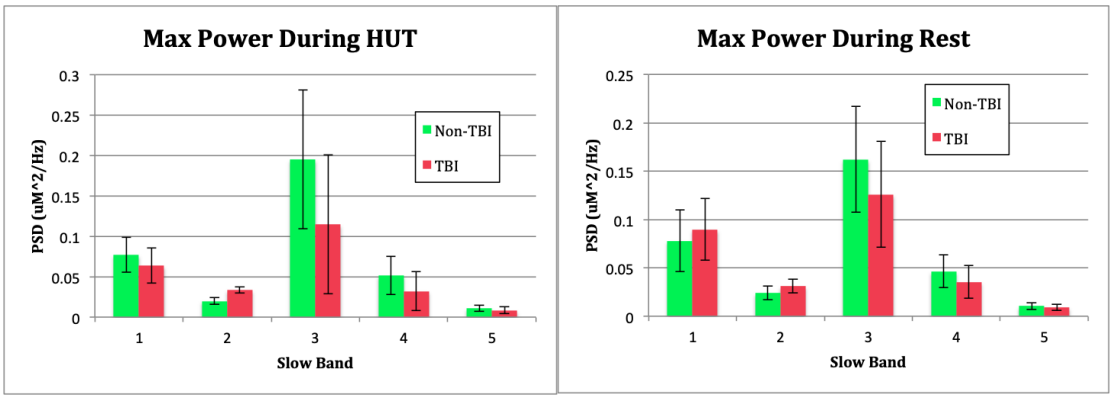

FIGURE 24: Comparison of max PSD of the non-TBI trials and TBI trials during (left) HUT and (right) the Rest position. These values can be found in Table 8 in the Appendix.

Regarding the HUT position, the non-TBI trials showed a higher maximum power than the TBI trials in all the slow bands except for the slow-2 band. Similarly in the resting position,

the non-TBI trials showed a higher maximum power in all the slow bands except for the slow-1 and slow-2 bands. By having higher maximum spontaneous activities within the slow-3, slow-4, and slow-5 bands in non-TBI trials at both HOB positions, these results convey that within these three slow bands, the uninjured brain has a stronger LFO response than the injured brain. This suggests that with injury comes a decrease in responsiveness for those three bands. Conversely, by having higher maximum powers within the slow-2 band in TBI trials at both HOB positions, these results convey that injury increases responsiveness of LFOs in the slow-4 band.

4. Limitations and Alternative Strategies

A limiting factor of this project was subject recruitment as it was on an opportunity basis for both populations. We were only able to recruit one TBI subject and performed measurements after the injury had occurred. Due to the limiting sample size of this group, we obtained three measurements from this same subject to represent the TBI population. The non-TBI control population was also obtained on an opportunity-basis, but due to higher sample-size, each control subject received one measurement. Therefore, this project serves to be descriptive and preliminary as a pilot study, rather than conclusive. It can be used as reference for future studies where increased subject recruitment would provide statistical power. To illustrate the limitation of this project to produce statistically conclusive results, a power analysis was conducted.

Power is defined as the probability of detecting a statistically significant difference given that the difference actually exists. The gold standard is 80% power, which was used in these power analyses. An overall level of significance of α=0.05 was used throughout. RStudio version 1.3.1073 was used for the analyses. Descriptive statistics by group are given below in **Table 1.**

TABLE 1: Descriptive statistics of hemodynamic concentration changes

Variable	Group	N	Mean	Std Dev	Minimum	Maximum
Change HbO	Non-TBI	12	0.49	0.58	-0.95	1.06
	TBI	3	0.34	-	-0.42	0.79
Change Hb	Non-TBI	12	-0.05	1.03	-1.53	1.75
	TBI	3	0.53	-	-0.87	2.43
Change THC	Non-TBI	12	0.44	0.59	-0.78	1.24
	TBI	3	0.87	-	-0.36	1.31

Since there was only one TBI patient, we cannot estimate the standard deviation for that group. Therefore, we must assume that the two groups have the same standard deviation, which may or may not be the case. This means the estimate for the non-TBI group was used as the estimate for the pooled standard deviation for both groups in the power analyses. However, there may be more variance in the TBI group, which means that the recommended sample sizes need to be larger than what are included in this power analysis. All power analyses are for independent samples t-tests.

The results of the power analysis are given in Table 2 below.

TABLE 2: Power analysis results

Variable	Group	Mean	Pooled S.D.	n per Group
Change HbO	Non-TBI	0.49	0.58	235
	TBI	0.34		
Change Hb	Non-TBI	-0.05	1.03	50
	TBI	0.53		
Change THC	Non-TBI	0.44	0.59	1116
	TBI	0.87		

The number of subjects per group needed to achieve 80% power from the statistics of this project is given in the far-right column. For example, the table indicates that 235 subjects per group (470 total subjects) are required to achieve 80% power for the change in HbO. Since we are taking the measurements from the same subjects, we would have to go with the largest sample size to achieve at least 80% power for all response variables. This means that we would need 1116 subjects per group (2232 total subjects from the Change THC variable), which was not feasible.

5. Conclusions & Future Work

Overall this project aimed to characterize the cerebral response of a non-TBI and a TBI population using frequency domain analysis of the fNIRS signal. Twelve non-TBI subjects underwent one optical measurement each and one TBI subject underwent three optical measurements of their DPFC following a HOB manipulation protocol.

In the time-domain, both groups showed an overall increase in HbO with HOB lowering, consistent with previous studies. Hb slightly decreased in the non-TBI group, but largely increased in the TBI group with HOB lowering. At the lower resting position, gravity no longer assists the brain with venous return and these concentration results show the effect of pooling. The TBI subject was significantly more affected by this than the non-TBI subjects and shows the potential effect of trauma on the brain's ability to autoregulate.

In the FD, we analyzed LFOs from the HbO time-domain signal. HbO was the hemodynamic parameter of choice for frequency analysis as it is representative of brain activity. In the HUT position, spontaneous oscillations around 0.1 Hz were present with similar magnitude in both study groups. This is consistent with previous studies identifying 0.1 Hz activity in the MAP and CBFV signals. This 0.1 Hz activity was also present in the resting position whereas in that previous study the resting position did not show 0.1 HZ LFO activity. Since their protocol began in the resting position and elevated their subjects, while this project began in HUT and then lowered subjects, 0.1 Hz might be more present at elevated positions and remain as a lingering mechanism in our project's resting measurements. LFOs near 0.027 Hz were present in the TBI group at the HUT position, but not in the non-TBI group or in either group at the resting position. Activity in a study on ASD children exhibited similar results suggesting this oscillation represents a

malfunctioning neurogenic mechanism observable at the HUT position. The ~0.027 Hz frequency, therefore becomes an identifiable feature of diseased brain states and should be followed up in subsequent studies, and the HUT position emerges as an ideal elevation under which to perform these measurements. A higher overall power in the HUT responses of the non-TBI group and more focused peaks also show the strength of using an elevated position when assessing LFO responses.

Previous studies have identified specific frequencies of interest when studying LFOs including 0.0133, 0.04, 0.067, 0.0933, and 0.1 Hz. This project also identified prevalence in the same LFOs of 0.0133, 0.08, 0.0933, and 0.1Hz. Additionally, 0.053 and 0.067 Hz were prevalent LFO peaks amongst subjects. These peaks also fall into ranges of LFOs called slow-bands that have been previously defined in a study[139]. We defined APIs as percent increases in power spectral density with the HUT position and APDs as percent decreases. Regarding average PSD, for non-TBI, APIs were more prevalent in the slow-3 and 5 bands, APDs in the slow-1 band, and equivalent occurrences of APIs and APDs in the slow-2 and 4 bands. In the TBI trials, all slow bands exhibited APDs. The overall average PSD change in each band (**Figure 19**) also showed percent decreases in all slow-bands in the TBI trials. This suggests, at least for the TBI subject in this project, that trauma causes decreased activity at the HUT position and shows the strength of using the HUT position when analyzing LFOs and characterizing TBI. This differentiation between non-TBI and TBI and consistency between APIs, APDs, and averaged PSDs was not as pronounced in the maximum analysis and therefore this project favors an analysis of average PSD within each band when studying cerebral response. Comparison of slow-bands between study groups was also possible with this analysis of average PSD within

each band. Regarding the HUT position, the non-TBI trials showed a higher power than the TBI trials in all the slow bands except for the slow-4 band. Similarly in the resting position, the non-TBI trials showed a higher power in all the slow bands except for the slow-4 and slow-5 bands. By having higher spontaneous activity of slow-1, slow-2, and slow-3 LFOs in non-TBI trials at both HOB positions, these results convey that within these three slow bands, the uninjured brain is more active than the injured brain in the mechanisms each of those bands represent. This suggests that with injury comes a decrease in activity for those three bands. Conversely, by having higher spontaneous activity of slow-4 LFOs in TBI trials at both HOB positions, and slow-5 in the resting position, these results convey that injury increases activity of the mechanism that the slow-4 band represents and slow-5 band at lowered positions. This is interesting as a previous study on preterm and term infants showed an inverse correlation between LFO activity and brain function[16]. Since the slow-4 and slow-5 bands have been shown to represent neurogenic and endothelial mechanisms respectively, this project consistently shows increased LFO response with inhibited brain function.

While this study used a time-series filter to individually assess LFOs at the HUT position and the Rest position, future studies could also look at the transition period to see if meaningful frequency or time domain information could characterize trauma in the brain as the elevation change is happening.

Finally, this project also showed the need of cerebral assessment to be taken on a case-by-case basis. Analyzing individual spectrums, subjects showed unique responses regardless of whether they were in the non-TBI or TBI group. The sole TBI subject who had three trials exhibited a similar response in all three measurements showing the

repeatability and precision of their cerebral assessment using fNIRS derived LFOs. This higher intersubject variability and lower intrasubject variability show the strength of individually assessing and characterizing cerebral response. Future studies should focus on recruiting more subjects and performing repeated measures to further validate this. However, this project illustrates the strength of a practical tool in fNIRS and assessment of LFOs to conveniently provide personalized assessment of unique cerebral response.

Bibliography

1. Blostein P, Jones SJ. Identification and evaluation of patients with mild traumatic brain injury: Results of a national survey of level i trauma centers. *J Trauma*. Published online 2003. doi:10.1097/01.TA.0000038545.24879.4D

2. Powell JM, Ferraro J V., Dikmen SS, Temkin NR, Bell KR. Accuracy of mild traumatic brain injury diagnosis. *Arch Phys Med Rehabil*. 2008;89(8):1550-1555. doi:10.1016/j.apmr.2007.12.035

3. Reith FCM, Lingsma HF, Gabbe BJ, Lecky FE, Roberts I, Maas AIR. Differential effects of the Glasgow Coma Scale Score and its Components: An analysis of 54,069 patients with traumatic brain injury $. *Int J Care Inj*. 2017;48:1932-1943. doi:10.1016/j.injury.2017.05.038

4. Katura T, Tanaka N, Obata A, Sato H, Maki A. Quantitative evaluation of interrelations between spontaneous low-frequency oscillations in cerebral hemodynamics and systemic cardiovascular dynamics. *Neuroimage*. 2006;31(4):1592-1600. doi:10.1016/j.neuroimage.2006.02.010

5. Heyl AG. The Calibre of the Retinal Vessels after Traumatic Injury to the Convexity of the Brain. *Trans Am Ophthalmol Soc*. 1891;6:190-200. Accessed February 7, 2021. http://www.ncbi.nlm.nih.gov/pubmed/25259113

6. Nolan S. Traumatic brain injury: A review. *Crit Care Nurs Q*. Published online 2005. doi:10.1097/00002727-200504000-00010

7. Blostein P, Jones SJ. Identification and evaluation of patients with mild traumatic brain injury: Results of a national survey of level i trauma centers. *J Trauma*. 2003;55(3):450-453. doi:10.1097/01.TA.0000038545.24879.4D

8. Gebke KB. Mild traumatic brain injury. *Curr Sports Med Rep*. Published online 2002. doi:10.1249/00149619-200202000-00005

9. Schleimer JA. Minor traumatic brain injury in sports. *Curr Sports Med Rep*. Published online 2002. doi:10.1249/00149619-200212000-00004

10. Eagle SR, Kontos AP, Collins MW, Connaboy C, Flanagan S. Network Analysis of Sport-related Concussion Research During the Past Decade (2010–2019). *J Athl Train*. Published online 2020. doi:10.4085/280-20

11. Bell JM, Breiding MJ, DePadilla L. CDC's efforts to improve traumatic brain injury surveillance. *J Safety Res*. 2017;62:253-256. doi:10.1016/j.jsr.2017.04.002

12. Laverse E, Guo T, Zimmerman K, et al. Plasma glial fibrillary acidic protein and neurofilament light chain, but not tau, are biomarkers of sports-related mild traumatic brain injury. *Brain Commun*. Published online 2020. doi:10.1093/braincomms/fcaa137

13. Zimmerman K, Kim J, Karton C, et al. Player position in American football influences the magnitude of mechanical strains produced in the location of chronic traumatic encephalopathy pathology: A computational modelling study. *J Biomech*. Published online 2021.

14. Shope C, Alshareef M, Larrew T, et al. Utility of a pediatric fast magnetic resonance imaging protocol as surveillance scanning for traumatic brain injury. *J Neurosurg Pediatr*. Published online 2021.

15. Kochanek PM, Tasker RC, Carney N, et al. Guidelines for the Management of Pediatric Severe Traumatic Brain Injury, Third Edition: Update of the Brain Trauma Foundation Guidelines,

Executive Summary. *Pediatr Crit Care Med*. Published online 2019. doi:10.1097/PCC.0000000000001736

16. Kato I, Kusaka T, Nishida T, et al. Extrauterine environment influences spontaneous low-frequency oscillations in the preterm brain. *Brain Dev*. 2013;35(1):17-25. doi:10.1016/j.braindev.2012.03.007

17. Terrio H, Brenner LA, Ivins BJ, et al. Traumatic brain injury screening: Preliminary findings in a US army brigade combat team. *J Head Trauma Rehabil*. Published online 2009. doi:10.1097/HTR.0b013e31819581d8

18. Singer K, Wallen T, Jalbert T, et al. Efficacy of Noninvasive Technologies in Triaging TBI and Correlating With ICP: A Prospective Study. *Surg Reseaarch*. 2021;(262):27-37.

19. Tolmacheva RA, Obukhov Y V., Zhavoronkova LA. The Estimation of Inter-Channel Phase Synchronization of EEG Signals in Patients with Traumatic Brain Injury Before and Post the Rehabilitation. In: *Advances in Intelligent Systems and Computing*. Vol 1255. Springer Science and Business Media Deutschland GmbH; 2021:511-520. doi:10.1007/978-981-15-7834-2_48

20. Arenth PM, Ricker JH, Schultheis MT. Applications of functional near-infrared spectroscopy (fNIRS) to neurorehabilitation of cognitive disabilities. *Clin Neuropsychol*. 2007;21(1):38-57. doi:10.1080/13854040600878785

21. Mukai K, Matsuura N, Miyauchi M, et al. Evaluation of hemodynamic changes using near-infrared spectroscopy in patients with tic-related obsessive-compulsive disorder. *Psychiatry Clin Neurosci*. Published online February 5, 2021:pcn.13207. doi:10.1111/pcn.13207

22. Skau S, Bunketorp-Käll L, Kuhn HG, Johansson B. Mental fatigue and functional near-infrared spectroscopy (fNIRS) – Based assessment of cognitive performance after mild traumatic brain injury. *Front Hum Neurosci*. 2019;13. doi:10.3389/fnhum.2019.00145

23. Merzagora AC, Schultheis MT, Onaral B, Izzetoglu M. Functional near-infrared spectroscopy-based assessment of attention impairments after traumatic brain injury. *J Innov Opt Health Sci*. 2011;4(3):251-260. doi:10.1142/S1793545811001551

24. Wu S, Cai S, Xiong G, et al. The only-child effect in the neural and behavioral signatures of trust revealed by fNIRS hyperscanning. *Brain Cogn*. 2021;149:105692. doi:10.1016/j.bandc.2021.105692

25. Li W, Qiu J, Li XL, et al. BBB pathophysiology–independent delivery of siRNA in traumatic brain injury. *Sci Adv*. 2021;7(1). doi:10.1126/sciadv.abd6889

26. Irimia A, Fan D, Chaudhari NN, et al. Mapping Cerebral Connectivity Changes after Mild Traumatic Brain Injury in Older Adults Using Diffusion Tensor Imaging and Riemannian Matching of Elastic Curves. In: *Proceedings - International Symposium on Biomedical Imaging*. Vol 2020-April. IEEE Computer Society; 2020:1690-1693. doi:10.1109/ISBI45749.2020.9098476

27. Shin SS, Huisman TAGM, Hwang M. Ultrasound imaging for traumatic brain injury. *J Ultrasound Med*. 2018;37(8):1857-1867. doi:10.1002/jum.14547

28. Amyot F, Zimmermann T, Riley J, et al. Normative database of judgment of complexity task with functional near infrared spectroscopy-Application for TBI. *Neuroimage*. 2012;60(2):879-883. doi:10.1016/j.neuroimage.2012.01.104

29. Karamzadeh N, Amyot F, Kenney K, et al. A machine learning approach to identify functional biomarkers in human prefrontal cortex for individuals with traumatic brain injury using functional near-infrared spectroscopy. *Brain Behav*. 2016;6(11). doi:10.1002/brb3.541

30. Cheng R, Shang Y, Hayes D, Saha SP, Yu G. Noninvasive optical evaluation of spontaneous low frequency oscillations in cerebral hemodynamics. *Neuroimage*. Published online 2012. doi:10.1016/j.neuroimage.2012.05.069

31. Reinhard M, Wehrle-Wieland E, Grabiak D, et al. Oscillatory cerebral hemodynamics-the macro- vs. microvascular level. *J Neurol Sci*. 2006;250(1-2):103-109. doi:10.1016/j.jns.2006.07.011

32. Heegaard W, Biros M. Traumatic Brain Injury. *Emerg Med Clin North Am*. Published online 2007. doi:10.1016/j.emc.2007.07.001

33. Salcido R, Costich JF. Recurrent traumatic brain injury. *Brain Inj*. Published online 1992. doi:10.3109/02699059209029671

34. Cuthbert JP, Harrison-Felix C, Corrigan JD, et al. Epidemiology of adults receiving acute inpatient rehabilitation for a primary diagnosis of traumatic brain injury in the United States. *J Head Trauma Rehabil*. 2015;30(2):122-135. doi:10.1097/HTR.0000000000000012

35. Frieden TR, Houry D, Baldwin G. Traumatic Brain Injury in the United States: Epidemiology and Rehabilitation. *CDC NIH Rep to Congr*. Published online 2015.

36. Xu LB, Yue JK, Korley F, et al. High-Sensitivity C-Reactive Protein Is a Prognostic Biomarker of Six-Month Disability after Traumatic Brain Injury: Results from the TRACK-TBI Study. *J Neurotrauma*. Published online 2020. doi:10.1089/neu.2020.7177

37. Adamovich-Zeitlin R, Wanda PA, Solomon E, et al. Biomarkers of memory variability in traumatic brain injury. *Brain Commun*. Published online 2020. doi:10.1093/braincomms/fcaa202

38. Okonkwo DO, Puffer RC, Puccio AM, et al. Point-of-Care Platform Blood Biomarker Testing of Glial Fibrillary Acidic Protein versus S100 Calcium-Binding Protein B for Prediction of Traumatic Brain Injuries: A Transforming Research and Clinical Knowledge in Traumatic Brain Injury Study. *J Neurotrauma*. 2020;37(23):2460-2467. doi:10.1089/neu.2020.7140

39. Michetti F, D'Ambrosi N, Toesca A, et al. The S100B story: from biomarker to active factor in neural injury. *J Neurochem*. 2019;148(2):168-187. doi:10.1111/jnc.14574

40. Gaetani L, Blennow K, Calabresi P, Di Filippo M, Parnetti L, Zetterberg H. Neurofilament light chain as a biomarker in neurological disorders. *J Neurol Neurosurg Psychiatry*. Published online 2019. doi:10.1136/jnnp-2018-320106

41. Vella MA, Crandall ML, Patel MB. Acute Management of Traumatic Brain Injury. *Surg Clin North Am*. Published online 2017. doi:10.1016/j.suc.2017.06.003

42. Hackenberg K, Unterberg A. Schädel-Hirn-Trauma. *Nervenarzt*. Published online 2016. doi:10.1007/s00115-015-0051-3

43. Stein DM, Feather CB, Napolitano LM. Traumatic Brain Injury Advances. *Crit Care Clin*. Published online 2017. doi:10.1016/j.ccc.2016.08.008

44. Sure U. Marc S. Greenberg: Handbook of neurosurgery, 6th edn. *Neurosurg Rev*. Published online 2007. doi:10.1007/s10143-006-0063-3

45. Araki T, Yokota H, Morita A. Pediatric traumatic brain injury: Characteristic features, diagnosis, and management. *Neurol Med Chir (Tokyo)*. Published online 2017. doi:10.2176/nmc.ra.2016-0191

46. Hawryluk GWJ, Aguilera S, Buki A, et al. A management algorithm for patients with intracranial pressure monitoring: the Seattle International Severe Traumatic Brain Injury Consensus Conference (SIBICC). In: *Intensive Care Medicine*. Vol 45. Springer; 2019:1783-1794. doi:10.1007/s00134-

019-05805-9

47. Chesnut R, Aguilera S, Buki A, et al. A management algorithm for adult patients with both brain oxygen and intracranial pressure monitoring: the Seattle International Severe Traumatic Brain Injury Consensus Conference (SIBICC). *Intensive Care Med*. 2020;46(5):919-929. doi:10.1007/s00134-019-05900-x

48. Silverberg D, Meer A, Silvinger E, Gross M, Feldman S. Head injuries after serious bicycle accidents. *Eur J Epidemiol*. Published online 1992. doi:10.1007/BF00145327

49. Joshipura M, Mock C, Goosen J, Peden M. Essential Trauma Care: Strengthening trauma systems round the world. In: *Injury*. ; 2004. doi:10.1016/j.injury.2003.08.005

50. Cuthbert JP, Harrison-Felix C, Corrigan JD, et al. Epidemiology of adults receiving acute inpatient rehabilitation for a primary diagnosis of traumatic brain injury in the United States. *J Head Trauma Rehabil*. Published online 2015. doi:10.1097/HTR.0000000000000012

51. Alverson C, Browne D, Dunn K, et al. Traumatic brain injury in the United States: A report to Congress. *Atlanta, GA Centers Dis Control Prev*. Published online 1999.

52. Jiang JY, Gao GY, Feng JF, et al. Traumatic brain injury in China. *Lancet Neurol*. 2019;18(3):286-295. doi:10.1016/S1474-4422(18)30469-1

53. Juul N, Morris GF, Marshall SB, Marshall LF. Intracranial hypertension and cerebral perfusion pressure: Influence on neurological deterioration and outcome in severe head injury. *J Neurosurg*. Published online 2000. doi:10.3171/jns.2000.92.1.0001

54. Sivakumar S, Taccone FS, Rehman M, Hinson H, Naval N, Lazaridis C. Hemodynamic and neuro-monitoring for neurocritically ill patients: An international survey of intensivists. *J Crit Care*. 2017;39:40-47. doi:10.1016/j.jcrc.2017.01.005

55. Vespa P, Tubi M, Claassen J, et al. Metabolic crisis occurs with seizures and periodic discharges after brain trauma. *Ann Neurol*. Published online 2016. doi:10.1002/ana.24606

56. Hartings JA, Andaluz N, Bullock MR, et al. Prognostic Value of Spreading Depolarizations in Patients with Severe Traumatic Brain Injury. *JAMA Neurol*. Published online 2020. doi:10.1001/jamaneurol.2019.4476

57. Steiner LA, Czosnyka M, Piechnik SK, et al. Continuous monitoring of cerebrovascular pressure reactivity allows determination of optimal cerebral perfusion pressure in patients with traumatic brain injury. *Crit Care Med*. Published online 2002. doi:10.1097/00003246-200204000-00002

58. Ghajar J. Traumatic brain injury. In: *Lancet*. ; 2000. doi:10.1016/S0140-6736(00)02689-1

59. Feldman Z, Kanter MJ, Robertson CS, et al. Effect of head elevation on intracranial pressure, cerebral perfusion pressure, and cerebral blood flow in head-injured patients. In: *Journal of Neurosurgery*. ; 1992. doi:10.3171/jns.1992.76.2.0207

60. Schulz-Stübner S, Thiex R. Raising the head-of-bed by 30 degrees reduces ICP and improves CPP without compromising cardiac output in euvolemic patients with traumatic brain injury and subarachnoid haemorrhage: A practice audit [3]. *Eur J Anaesthesiol*. 2006;23(2):177-180. doi:10.1017/S0265021505232118

61. Lang SS, Valeri A, Zhang B, et al. Head of bed elevation in pediatric patients with severe traumatic brain injury. *J Neurosurg Pediatr*. 2020;26(5):465-475. doi:10.3171/2020.4.PEDS20102

62. Freeman WD. Management of intracranial pressure. *Contin Lifelong Learn Neurol*.

2015;21(5):1299-1323. doi:10.1212/CON.0000000000000235

63. Stiefel MF, Spiotta A, Gracias VH, et al. Reduced mortality rate in patients with severe traumatic brain injury treated with brain tissue oxygen monitoring. *J Neurosurg*. 2005;103(5):805-811. doi:10.3171/jns.2005.103.5.0805

64. Cold GE, Jensen FT. Cerebral Autoregulation in Unconscious Patients with Brain Injury. *Acta Anaesthesiol Scand*. Published online 1978. doi:10.1111/j.1399-6576.1978.tb01301.x

65. Skyhøj Olsen T, Larsen B, Bech Skriver E, Enevoldsen E, Lassen NA. Focal cerebral ischemia measured by the intra-arterial 133xenon method. Limitations of 2-dimensional blood flow measurements. *Stroke*. Published online 1981. doi:10.1161/01.str.12.6.736

66. Bourel-Ponchel E, Mahmoudzadeh M, Delignières A, Berquin P, Wallois F. Non-invasive, multimodal analysis of cortical activity, blood volume and neurovascular coupling in infantile spasms using EEG-fNIRS monitoring. *NeuroImage Clin*. 2017;15:359-366. doi:10.1016/j.nicl.2017.05.004

67. Standvoss K, Goerke L, Crijns T, et al. Cerebral microbleed detection in traumatic brain injury patients using 3D convolutional neural networks. In: *Progress in Biomedical Optics and Imaging - Proceedings of SPIE*. Vol v 10575. SPIE-Intl Soc Optical Eng; 2018:48. doi:10.1117/12.2294016

68. Ludewig P, Gdaniec N, Sedlacik J, et al. Magnetic Particle Imaging for Real-Time Perfusion Imaging in Acute Stroke. *ACS Nano*. Published online 2017. doi:10.1021/acsnano.7b05784

69. Orendorff R, Peck AJ, Zheng B, et al. First in vivo traumatic brain injury imaging via magnetic particle imaging. *Phys Med Biol*. Published online 2017. doi:10.1088/1361-6560/aa52ad

70. Wu XLC, Zhang XY, Steinberg XG, et al. A review of magnetic particle imaging and perspectives on neuroimaging. *Am J Neuroradiol*. 2019;40(2):206-212. doi:10.3174/ajnr.A5896

71. Schell RM, Cole DJ. Cerebral Monitoring: Jugular Venous Oximetry. *Anesth Analg*. 2000;90(3):559-566. doi:10.1097/00000539-200003000-00012

72. Foreman B, Lissak IA, Kamireddi N, Moberg D, Rosenthal ES. Challenges and Opportunities in Multimodal Monitoring and Data Analytics in Traumatic Brain Injury. *Curr Neurol Neurosci Rep*. 2021;21(3):6. doi:10.1007/s11910-021-01098-y

73. Behrens A, Lenfeldt N, Ambarki K, Malm J, Eklund A, Koskinen LO. Transcranial doppler pulsatility index: Not an accurate method to assess intracranial pressure. *Neurosurgery*. 2010;66(6):1050-1057. doi:10.1227/01.NEU.0000369519.35932.F2

74. Figaji AA, Zwane E, Fieggen AG, Siesjo P, Peter JC. Transcranial Doppler pulsatility index is not a reliable indicator of intracranial pressure in children with severe traumatic brain injury. *Surg Neurol*. 2009;72(4):389-394. doi:10.1016/j.surneu.2009.02.012

75. Sirpal P, Kassab A, Pouliot P, Nguyen DK. fNIRS improves seizure detection in multimodal EEG-fNIRS recordings. *J Biomed Opt*. Published online 2019. doi:10.1117/1.jbo.24.5.051408

76. Len-Carrin J, Len-Domnguez U. Functional Near-Infrared Spectroscopy (fNIRS): Principles and Neuroscientific Applications. In: *Neuroimaging - Methods*. InTech; 2012. doi:10.5772/23146

77. Yu Y, Hou K, Ji T, et al. The role of exosomal microRNAs in central nervous system diseases. *Mol Cell Biochem*. Published online January 29, 2021:1-14. doi:10.1007/s11010-021-04053-0

78. Kudryashev JA, Waggoner LE, Leng HT, Mininni NH, Kwon EJ. An Activity-Based Nanosensor for Traumatic Brain Injury. *ACS Sensors*. 2020;5(3):686-692. doi:10.1021/acssensors.9b01812

79. Perutz MF. Nature of haem-haem interaction. *Nature*. 1972;237(5357):495-499. doi:10.1038/237495a0

80. Jöbsis FF. Noninvasive, infrared monitoring of cerebral and myocardial oxygen sufficiency and circulatory parameters. *Science (80-).* 1977;198(4323):1264-1266. doi:10.1126/science.929199

81. Boas DA, Elwell CE, Ferrari M, Taga G. Twenty years of functional near-infrared spectroscopy: Introduction for the special issue. *Neuroimage*. 2014;85:1-5. doi:10.1016/j.neuroimage.2013.11.033

82. Hall JW, Pollard A. Near-infrared spectrophotometry: A new dimension in clinical chemistry. In: *Clinical Chemistry*. Vol 38. ; 1992:1623-1631. doi:10.1093/clinchem/38.9.1623

83. Watanabe S, Ishii C, Takeyasu N, et al. Assessing muscle vasodilation using near-infrared spectroscopy in cardiac patients. *Circ J*. 2005;69(7):802-814. doi:10.1253/circj.69.802

84. Hammer SM, Alexander AM, Didier KD, et al. The noninvasive simultaneous measurement of tissue oxygenation and microvascular hemodynamics during incremental handgrip exercise. *J Appl Physiol*. 2018;124(3):604-614. doi:10.1152/japplphysiol.00815.2017

85. Ferreira LF, Koga S, Barstow TJ. Dynamics of noninvasively estimated microvascular O2 extraction during ramp exercise. *J Appl Physiol*. 2007;103(6):1999-2004. doi:10.1152/japplphysiol.01414.2006

86. Bendahan D, Chatel B, Jue T. Comparative NMR and NIRS analysis of oxygen-dependent metabolism in exercising finger flexor muscles. *Am J Physiol - Regul Integr Comp Physiol*. 2017;313(6):R740-R753. doi:10.1152/ajpregu.00203.2017

87. Lynch Gwen Lech DR, Farmer JM, Balcer LJ, Bank W, Chance B, Wilson RB. Near infrared muscle spectroscopy in patients with Friedreich's ataxia. *Muscle and Nerve*. 2002;25(5):664-673. doi:10.1002/mus.10077

88. Bank W, Chance B. An oxidative defect in metabolic myopathies: Diagnosis by noninvasive tissue oximetry. *Ann Neurol*. 1994;36(6):830-837. doi:10.1002/ana.410360606

89. Lauridsen RK, Everland H, Nielsen LF, Engelsen SB, Nørgaard L. Exploratory multivariate spectroscopic study on human skin. *Ski Res Technol*. 2003;9(2):137-146. doi:10.1034/j.1600-0846.2003.00014.x

90. Ali JH, Wang WB, Zevallos M, Alfano RR. Near infrared spectroscopy and imaging to probe differences in water content in normal and cancer human prostate tissues. *Technol Cancer Res Treat*. 2004;3(5):491-497. doi:10.1177/153303460400300510

91. Hirosawa N, Sakamoto Y, Katayama H, Tonooka S, Yano K. In vivo investigation of progressive alterations in rat mammary gland tumors by near-infrared spectroscopy. *Anal Biochem*. 2002;305(2):156-165. doi:10.1006/abio.2002.5649

92. Liu J, Han J, Kang Z, et al. In vivo near-infrared photothermal therapy and computed tomography imaging of cancer cells using novel tungsten-based theranostic probe. *Nanoscale*. 2014;6(11):5770-5776. doi:10.1039/c3nr06292a

93. Ben Mohammadi L, Klotzbuecher T, Sigloch S, et al. In vivo evaluation of a chip based near infrared sensor for continuous glucose monitoring. *Biosens Bioelectron*. 2014;53:99-104. doi:10.1016/j.bios.2013.09.043

94. Heise HM, Marbach R, Koschinsky T, Gries FA. Noninvasive Blood Glucose Sensors Based on Near-Infrared Spectroscopy. *Artif Organs*. 1994;18(6):439-447. doi:10.1111/j.1525-

1594.1994.tb02230.x

95. Maruo K, Tsurugi M, Tamura M, Ozaki Y. In Vivo Noninvasive Measurement of Blood Glucose by Near-Infrared Diffuse-Reflectance Spectroscopy. *Appl Spectrosc*. 2003;57(10):1236-1244. doi:10.1366/000370203769699090

96. Gabriely I, Wozniak R, Mevorach M, Kaplan J, Aharon Y, Shamoon H. Transcutaneous glucose measurement using near-infrared spectroscopy during hypoglycemia. *Diabetes Care*. 1999;22(12):2026-2032. doi:10.2337/diacare.22.12.2026

97. Robinson MR, Eaton RP, Haaland DM, et al. Noninvasive glucose monitoring in diabetic patients: A preliminary evaluation. *Clin Chem*. 1992;38(9):1618-1622. doi:10.1093/clinchem/38.9.1618

98. Okada F, Tokumitsu Y, Hoshi Y, Tamura M. Impaired interhemispheric integration in brain oxygenation and hemodynamics in schizophrenia. *Eur Arch Psychiatry Clin Neurosci*. Published online 1994. doi:10.1007/BF02279807

99. Shinba T, Nagano M, Kariya N, et al. Near-infrared spectroscopy analysis of frontal lobe dysfunction in schizophrenia. *Biol Psychiatry*. Published online 2004. doi:10.1016/S0006-3223(03)00547-X

100. Suto T, Fukuda M, Ito M, Uehara T, Mikuni M. Multichannel near-infrared spectroscopy in depression and schizophrenia: Cognitive brain activation study. *Biol Psychiatry*. Published online 2004. doi:10.1016/j.biopsych.2003.09.008

101. Takizawa R, Kasai K, Kawakubo Y, et al. Reduced frontopolar activation during verbal fluency task in schizophrenia: A multi-channel near-infrared spectroscopy study. *Schizophr Res*. Published online 2008. doi:10.1016/j.schres.2007.10.025

102. Kubota Y, Toichi M, Shimizu M, et al. Prefrontal activation during verbal fluency tests in schizophrenia - A near-infrared spectroscopy (NIRS) study. *Schizophr Res*. Published online 2005. doi:10.1016/j.schres.2005.01.007

103. Hock C, Villringer K, Müller-Spahn F, et al. Near infrared spectroscopy in the diagnosis of Alzheimer's disease. In: *Annals of the New York Academy of Sciences*. Vol 777. Blackwell Publishing Inc.; 1996:22-29. doi:10.1111/j.1749-6632.1996.tb34397.x

104. Chou PH, Lan TH. The role of near-infrared spectroscopy in Alzheimer's disease. *J Clin Gerontol Geriatr*. Published online 2013. doi:10.1016/j.jcgg.2013.01.002

105. Shinoura N, Yamada R. Decreased vasoreactivity to right cerebral hemisphere pressure in migraine without aura: A near-infrared spectroscopy study. *Clin Neurophysiol*. 2005;116(6):1280-1285. doi:10.1016/j.clinph.2005.01.016

106. Thiagarajah JR, Papadopoulos MC, Verkman AS. Noninvasive early detection of brain edema in mice by near-infrared light scattering. *J Neurosci Res*. 2005;80(2):293-299. doi:10.1002/jnr.20439

107. Miki A, Nakajima T, Takagi M, et al. Near-infrared spectroscopy of the visual cortex in unilateral optic neuritis. *Am J Ophthalmol*. 2005;139(2):353-356. doi:10.1016/j.ajo.2004.07.042

108. Pinna V, Doneddu A, Roberto S, et al. Combined mental task and metaboreflex impair cerebral oxygenation in patients with type 2 Diabetes Mellitus. *Am J Physiol Regul Integr Comp Physiol*. Published online February 3, 2021:ajpregu.00288.2020. doi:10.1152/ajpregu.00288.2020

109. Kashiwagi S, Yuan J, Forbes B, et al. Near-infrared laser adjuvant for influenza vaccine. *PLoS One*. 2013;8(12). doi:10.1371/journal.pone.0082899

110. Meek JH, Firbank M, Elwell CE, Atkinson J, Braddick O, Wyatt JS. Regional hemodynamic responses to visual stimulation in awake infants. *Pediatr Res*. Published online 1998. doi:10.1203/00006450-199806000-00019

111. Lloyd-Fox S, Blasi A, Elwell CE. Illuminating the developing brain: The past, present and future of functional near infrared spectroscopy. *Neurosci Biobehav Rev*. Published online 2010. doi:10.1016/j.neubiorev.2009.07.008

112. Ghosh A, Elwell C, Smith M. Cerebral near-infrared spectroscopy in adults: A work in progress. *Anesth Analg*. 2012;115(6):1373-1383. doi:10.1213/ANE.0b013e31826dd6a6

113. Ferrari M. Progress of near-infrared spectroscopy and topography for brain and muscle clinical applications. *J Biomed Opt*. 2007;12(6):062104. doi:10.1117/1.2804899

114. Soekadar SR, Kohl SH, Mihara M, von Lühmann A. Optical brain imaging and its application to neurofeedback. *NeuroImage Clin*. 2021;30. doi:10.1016/j.nicl.2021.102577

115. Germon TJ, Kane NM, Manara AR, Nelson RJ. Near-infrared spectroscopy in adults: Effects of extracranial ischaemia and intracranial hypoxia on estimation of cerebral oxygenation. *Br J Anaesth*. 1994;73(4):503-506. doi:10.1093/bja/73.4.503

116. Davies DJ, Su Z, Clancy MT, et al. Near-Infrared Spectroscopy in the Monitoring of Adult Traumatic Brain Injury: A Review. *J Neurotrauma*. 2015;32(13):933-941. doi:10.1089/neu.2014.3748

117. Budohoski KP, Zweifel C, Kasprowicz M, et al. What comes first? the dynamics of cerebral oxygenation and blood flow in response to changes in arterial pressure and intracranial pressure after head injury. *Br J Anaesth*. 2012;108(1):89-99. doi:10.1093/bja/aer324

118. Weerakkody RA, Czosnyka M, Zweifel C, et al. Near infrared spectroscopy as possible non-invasive monitor of slow vasogenic ICP waves. In: *Acta Neurochirurgica, Supplementum*. Vol 114. Springer-Verlag Wien; 2012:181-185. doi:10.1007/978-3-7091-0956-4_35

119. Gibson AP, Hebden JC, Arridge SR. Recent advances in diffuse optical imaging. *Phys Med Biol*. 2005;50(4):1-43. doi:10.1088/0031-9155/50/4/R01

120. Zhang J, Zhang J, Ren H, et al. A Look Into the Power of fNIRS Signals by Using the Welch Power Spectral Estimate for Deception Detection. *Front Hum Neurosci*. 2020;14:606238. doi:10.3389/fnhum.2020.606238

121. Holmes O, Houchin J. Units in the cerebral cortex of the anaesthetized rat and the correlations between their discharges. *J Physiol*. 1966;187(3):651-671. doi:10.1113/jphysiol.1966.sp008116

122. Buzsáki G, Logothetis N, Singer W. Scaling brain size, keeping timing: Evolutionary preservation of brain rhythms. *Neuron*. 2013;80(3):751-764. doi:10.1016/j.neuron.2013.10.002

123. Henry JC. Electroencephalography: Basic Principles, Clinical Applications, and Related Fields, Fifth Edition. *Neurology*. 2006;67(11):2092-2092. doi:10.1212/01.wnl.0000243257.85592.9a

124. Obrig H, Neufang M, Wenzel R, et al. Spontaneous low frequency oscillations of cerebral hemodynamics and metabolism in human adults. *Neuroimage*. Published online 2000. doi:10.1006/nimg.2000.0657

125. Van Beek AHEA, Claassen JAHR, Rikkert MGMO, Jansen RWMM. Cerebral autoregulation: An overview of current concepts and methodology with special focus on the elderly. *J Cereb Blood Flow Metab*. 2008;28(6):1071-1085. doi:10.1038/jcbfm.2008.13

126. Sassaroli A, Pierro M, Bergethon PR, Fantini S. Low-frequency spontaneous oscillations of cerebral hemodynamics investigated with near-infrared spectroscopy: A review. *IEEE J Sel Top Quantum Electron*. 2012;18(4):1478-1492. doi:10.1109/JSTQE.2012.2183581

127. Steriade M, McCormick DA, Sejnowski TJ. Thalamocortical oscillations in the sleeping and aroused brain. *Science (80-)*. 1993;262(5134):679-685. doi:10.1126/science.8235588

128. Rusinov VS, Grindel' OM, Sharova E V., Kulikov MA, Kaliuzhnyĭ VN. Nizkochastotnaia sostavliaiushchaia EEG zdorovogo cheloveka i ee izmeneniia pod vliianiem ostro razvivaiushchikhsia ochagov na urovne dientsefal'nykh i stvolovykh struktur. *Zhurnal Vyss Nervn Deyatelnosti Im IP Pavlov*. 1988;38(2):207-218. Accessed February 6, 2021. https://pubmed-ncbi-nlm-nih-gov.ezproxy.libraries.wright.edu/3400316/

129. Hodkinson DJ, Wilcox SL, Veggeberg R, et al. Increased amplitude of thalamocortical low-frequency oscillations in patients with migraine. *J Neurosci*. 2016;36(30):8026-8036. doi:10.1523/JNEUROSCI.1038-16.2016

130. Biswal B, Zerrin Yetkin F, Haughton VM, Hyde JS. Functional connectivity in the motor cortex of resting human brain using echo-planar mri. *Magn Reson Med*. 1995;34(4):537-541. doi:10.1002/mrm.1910340409

131. Fox MD, Raichle ME. Spontaneous fluctuations in brain activity observed with functional magnetic resonance imaging. *Nat Rev Neurosci*. 2007;8(9):700-711. doi:10.1038/nrn2201

132. Buzsáki G, Draguhn A. Neuronal olscillations in cortical networks. *Science (80-)*. 2004;304(5679):1926-1929. doi:10.1126/science.1099745

133. Vanhatalo S, Palva JM, Holmes MD, Miller JW, Voipio J, Kaila K. Infraslow oscillations modulate excitability and interictal epileptic activity in the human cortex during sleep. *Proc Natl Acad Sci U S A*. 2004;101(14):5053-5057. doi:10.1073/pnas.0305375101

134. Bruns A, Eckhorn R, Jokeit H, Ebner A. Amplitude envelope correlation detects coupling among incoherent brain signals. *Neuroreport*. 2000;11(7):1509-1514. doi:10.1097/00001756-200005150-00029

135. Chan RW, Leong ATL, Ho LC, et al. Low-frequency hippocampal–cortical activity drives brain-wide resting-state functional MRI connectivity. *Proc Natl Acad Sci U S A*. 2017;114(33):E6972-E6981. doi:10.1073/pnas.1703309114

136. Zhang B, Jung M, Tu Y, et al. Identifying brain regions associated with the neuropathology of chronic low back pain: a resting-state amplitude of low-frequency fluctuation study. *Br J Anaesth*. 2019;123(2):e303-e311. doi:10.1016/j.bja.2019.02.021

137. Gao Q, Peng B, Huang X, et al. Assessment of cerebral low-frequency oscillations in patients with retinal vein occlusion: a preliminary functional MRI study. *Acta radiol*. 2020;61(6):813-820. doi:10.1177/0284185119879683

138. Yu Y, Chen L, Wang Q, et al. Altered amplitude of low-frequency fluctuations in inactive patients with nonneuropsychiatric systemic lupus erythematosus. *Neural Plast*. 2019;2019. doi:10.1155/2019/9408612

139. Zhan J, Gao L, Zhou F, et al. Amplitude of low-frequency fluctuations in multiple-frequency bands in acute mild traumatic brain injury. *Front Hum Neurosci*. 2016;10(FEB2016). doi:10.3389/fnhum.2016.00027

140. Chernomordik V, Amyot F, Kenney K, Wassermann E, Diaz-Arrastia R, Gandjbakhche A. Abnormality of low frequency cerebral hemodynamics oscillations in TBI population. *Brain Res*.

2016;1639:194-199. doi:10.1016/j.brainres.2016.02.018

141. Leung TS, Tisdall MM, Tachtsidis I, Smith M, Delpy DT, Elwell CE. Cerebral tissue oxygen saturation calculated using low frequency haemoglobin oscillations measured by near infrared spectroscopy in adult ventilated patients. In: *Advances in Experimental Medicine and Biology*. Vol 614. Springer New York; 2008:235-244. doi:10.1007/978-0-387-74911-2_27

142. Chen G, Popa LS, Wang X, et al. Low-frequency oscillations in the cerebellar cortex of the tottering mouse. *J Neurophysiol*. 2009;101(1):234-245. doi:10.1152/jn.90829.2008

143. ISS Inc. (2008). Oxiplex TS Operation Manual (01st ed., Vol. M03, Ser. 01). Champaign, IL.

144. Cheng, H., Yu, J., Xu, L., & Li, J. (2019). Power spectrum of spontaneous cerebral homodynamic oscillation shows a distinct pattern in autism spectrum disorder. *Biomedical Optics Express*. https://doi.org/10.1364/boe.10.001383

143. Kim, M. N., Edlow, B. L., Durduran, T., Frangos, S., Mesquita, R. C., Levine, J. M., … Detre, J. A. (2013). Continuous Optical Monitoring of Cerebral Hemodynamics During Head-of-Bed Manipulation in Brain-Injured Adults. Neurocritical Care, 20(3), 443–453. https://doi.org/10.1007/s12028-013-9849-7

Appendix

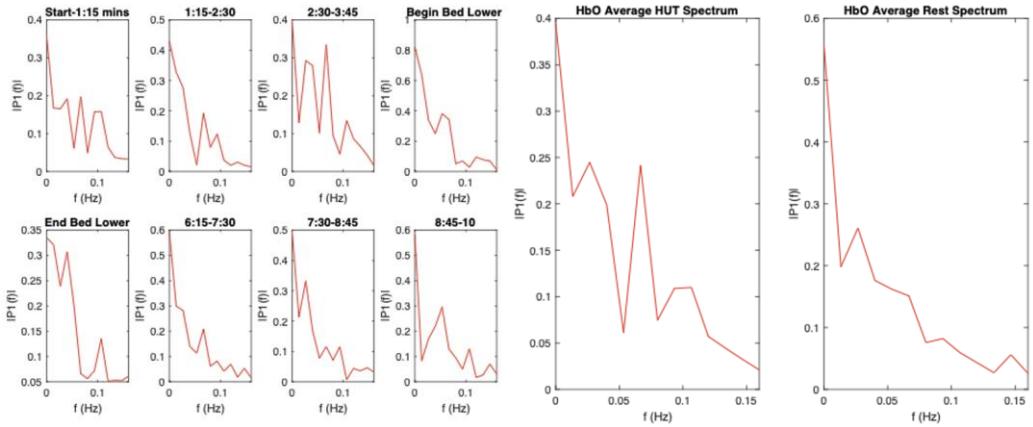

FIGURE 25: Example FD series of a non-TBI trial's HbO LFO spectrum used in the frequency prevalence analysis. (Left) Time progression of the frequency spectrums including two plots with transition periods and (Right) the time-series filtered frequency spectrums that were used to isolate frequency peaks. A frequency was considered a peak if its PSD magnitude was greater than the value of its neighboring observations.

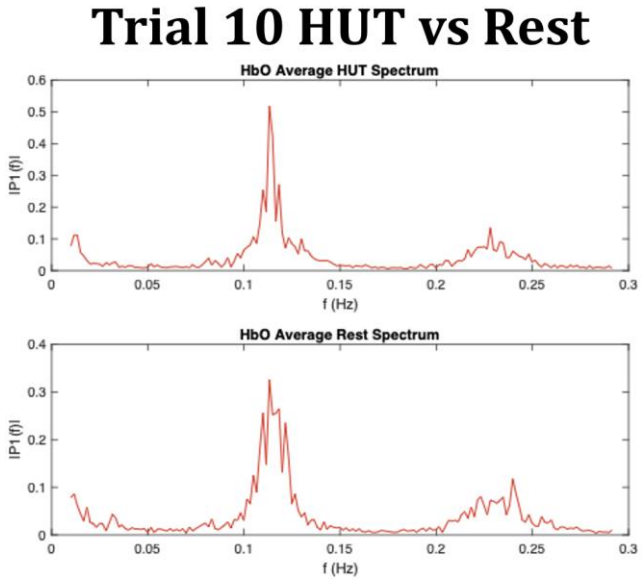

FIGURE 26: Example of an individual HbO spectrum at the two HOB positions.

TABLE 3: The average power spectrum densities in units of uM^2/Hz for each trial at each HOB elevation.

Trial	Slow-1 Avg. PSD HUT	Slow-2 Avg. PSD HUT	Slow-3 Avg. PSD HUT	Slow-4 Avg. PSD HUT	Slow-5 Avg. PSD HUT
Healthy 1	0.0058533	0.012077	0.026786	0.01099	0.024086

Healthy 2	0.0024063	0.0058102	0.021885	0.0089512	0.022026
Healthy 3	0.0020352	0.0055107	0.01815	0.0052627	0.033223
Healthy 4	0.00396	0.0060064	0.014461	0.011459	0.04184
Healthy 5	0.0012505	0.0021719	0.007388	0.0057976	0.025077
Healthy 6	0.0024371	0.0030778	0.006882	0.0050882	0.013444
Healthy 7	0.0022502	0.004942	0.013651	0.0035232	0.015635
Healthy 8	0.01034	0.022011	0.070983	0.018578	0.058443
Healthy 9	0.0049748	0.0073331	0.02032	0.011379	0.03717
Healthy 10	0.011716	0.024548	0.05477	0.01374	0.045818
Healthy 11	0.0084212	0.013986	0.041189	0.011197	0.054012
Healthy 12	0.00528	0.0067909	0.014356	0.0095878	0.025711
TBI 1	0.0088066	0.014211	0.035764	0.024851	0.04967
TBI 2	0.0033963	0.0056459	0.013926	0.008314	0.018306
TBI 3	0.0014711	0.0022196	0.0087932	0.0069216	0.019034

Trial	**Slow-1 Avg. PSD Rest**	**Slow-2 Avg. PSD Rest**	**Slow-3 Avg. PSD Rest**	**Slow-4 Avg. PSD Rest**	**Slow-5 Avg. PSD Rest**
Healthy 1	0.0052053	0.0094206	0.021271	0.010756	0.011587
Healthy 2	0.0025979	0.006307	0.021258	0.0071588	0.030599
Healthy 3	0.0024101	0.0062453	0.018104	0.0050307	0.031032
Healthy 4	0.0045794	0.0080672	0.019969	0.010398	0.035294
Healthy 5	0.0013517	0.0023778	0.0070394	0.005089	0.016392
Healthy 6	0.0026072	0.0029779	0.0060811	0.005621	0.011715
Healthy 7	0.0023126	0.0044226	0.011918	0.010126	0.027803
Healthy 8	0.0046608	0.015042	0.044635	0.018773	0.061069
Healthy 9	0.0054107	0.0071578	0.016734	0.0096799	0.02805
Healthy 10	0.011633	0.02326	0.049115	0.014043	0.039184
Healthy 11	0.010157	0.019949	0.05738	0.017124	0.12825
Healthy 12	0.0055259	0.0090585	0.022916	0.010478	0.023282
TBI 1	0.0092678	0.016086	0.040203	0.02664	0.072887
TBI 2	0.0036188	0.0060917	0.01946	0.013841	0.051721
TBI 3	0.0015433	0.0027913	0.011133	0.0077034	0.02378

TABLE 4: The percent change of average PSD defined as 100 x ($PSD_{HUT} - PSD_{REST}$)/ PSD_{REST} for each trial. This metric was used to assess the effects of HOB manipulation in the non-TBI and TBI trials.

Trial	**% Change Slow-1**	**% Change Slow-2**	**% Change Slow-3**	**% Change Slow-4**	**% Change Slow-5**
Healthy 1	362.7206885	28.19777933	25.92731888	2.175529937	107.8708898
Healthy 2	-7.375187652	-7.876962106	2.949477844	25.03771582	-28.01725547
Healthy 3	-15.55537115	-11.76244536	0.254087494	4.611684259	7.060453725

Healthy 4	-13.5257894	-25.54541848	-27.58275327	10.20388536	18.54706182
Healthy 5	-7.486868388	-8.659264867	4.952126602	13.92415013	52.98316252
Healthy 6	-6.524240565	3.354713053	13.17031458	-9.478740438	14.75885617
Healthy 7	-2.698261697	11.74422286	14.54103037	-65.20639937	-43.76506132
Healthy 8	121.8503261	46.33027523	59.02990926	-1.03872583	-4.300054037
Healthy 9	-8.056258894	2.449076532	21.42942512	17.55286728	32.51336898
Healthy 10	0.713487492	5.537403267	11.51379416	-2.15765862	16.93037975
Healthy 11	-17.08969184	-29.89122262	-28.21714883	-34.61224013	-57.88538012
Healthy 12	-4.449953854	-25.03284208	-37.35381393	-8.495896163	10.4329525
TBI 1	-4.976369796	-11.65609847	-11.04146457	-6.715465465	-31.85341693
TBI 2	-6.148446999	-7.31815421	-28.43782117	-39.93208583	-64.60625278
TBI 3	-4.678286788	-20.48149608	-21.01679691	-10.14876548	-19.95794786

TABLE 5: Average power spectrum densities (PSDs) in units of uM^2/Hz of the non-TBI trials and TBI trials during HUT and the Rest position.

Study Group & Elevation	Average PSD Slow-1	Average PSD Slow-2	Average PSD Slow-3	Average PSD Slow-4	Average PSD Slow-5
non-TBI HUT	0.00507705	0.009522083	0.02590175	0.009629475	0.033040417
TBI HUT	0.004558	0.007358833	0.0194944	0.0133622	0.029003333
non-TBI Rest	0.004870967	0.009523808	0.024701708	0.01035645	0.037021417
TBI Rest	0.004809967	0.008323	0.023598667	0.016061467	0.049462667

TABLE 6: The max power spectrum densities in units of uM^2/Hz for each trial at each HOB elevation.

Trial	Slow-1 Max PSD HUT	Slow-2 Max PSD HUT	Slow-3 Max PSD HUT	Slow-4 Max PSD HUT	Slow-5 Max PSD HUT
Healthy 1	0.041415441	0.030897162	0.34953747	0.105975573	0.015210128
Healthy 2	0.046493474	0.021613898	0.158180259	0.031468553	0.00459418
Healthy 3	0.107250112	0.010878272	0.147688067	0.026289532	0.004097818
Healthy 4	0.09688213	0.017249898	0.055350267	0.015106703	0.007177779
Healthy 5	0.048869434	0.01210692	0.05492372	0.012695942	0.002492808
Healthy 6	0.021572006	0.01155927	0.036655193	0.008961974	0.004390495
Healthy 7	0.043512274	0.008192022	0.0790534	0.026031644	0.005071375
Healthy 8	0.152269569	0.032282062	0.475013974	0.12666653	0.026272386
Healthy 9	0.063140951	0.020043941	0.088018456	0.022254097	0.00842813
Healthy 10	0.112594479	0.026879262	0.51825385	0.13530751	0.023828847
Healthy 11	0.141450972	0.026319692	0.303309593	0.087426789	0.020715698
Healthy 12	0.050570005	0.020989033	0.077549801	0.020352816	0.009134317
TBI 1	0.097807968	0.058707282	0.193982	0.066783012	0.015563387
TBI 2	0.037529432	0.017481989	0.08520546	0.021027168	0.00634762

TBI 3	0.05549432	0.024602707	0.064468184	0.008191126	0.003002197

Trial	Slow-1 Max PSD Rest	Slow-2 Max PSD Rest	Slow-3 Max PSD Rest	Slow-4 Max PSD Rest	Slow-5 Max PSD Rest
Healthy 1	0.019371803	0.024928405	0.221804376	0.065167661	0.012919589
Healthy 2	0.071576576	0.02065786	0.13104969	0.029394198	0.005146889
Healthy 3	0.097851659	0.008208015	0.131272694	0.038761062	0.005226595
Healthy 4	0.077094575	0.018151697	0.089058089	0.026637084	0.009005438
Healthy 5	0.036203851	0.014213541	0.042873863	0.012714772	0.002313103
Healthy 6	0.018880242	0.011741398	0.03402787	0.008742026	0.004612373
Healthy 7	0.052467942	0.015593188	0.070118501	0.017461129	0.004142972
Healthy 8	0.115159437	0.030558672	0.315033963	0.083073291	0.015596904
Healthy 9	0.060955082	0.01773255	0.080059354	0.020066955	0.011149166
Healthy 10	0.086127916	0.043432042	0.325307132	0.118047834	0.025002175
Healthy 11	0.256871271	0.056429396	0.319436409	0.074081312	0.018095973
Healthy 12	0.039948889	0.026625947	0.184766811	0.060543868	0.010736774
TBI 1	0.123055108	0.052320538	0.243364557	0.073483686	0.017277063
TBI 2	0.096354686	0.023335007	0.073425327	0.020226078	0.007140776
TBI 3	0.049700692	0.01736448	0.06066677	0.012325084	0.002803348

TABLE 7: The percent change of max PSD defined as 100 x ($PSD_{HUT} - PSD_{REST}$)/ PSD_{REST} for each trial. This metric was used to assess the effects of HOB manipulation in the non-TBI and TBI trials.

Trial	% Change Slow-1	% Change Slow-2	% Change Slow-3	% Change Slow-4	% Change Slow-5
Healthy 1	113.7923863	23.94360005	57.58817583	62.61988155	17.72918915
Healthy 2	-35.04373008	4.62796245	20.70250557	7.057020718	-10.73868782
Healthy 3	9.604796381	32.53229904	12.50478814	-32.17540796	-21.59678548
Healthy 4	25.66659844	-4.968127044	-37.84925396	-43.28694829	-20.29505336
Healthy 5	34.98407656	-14.82122986	28.10536743	-0.148093478	7.769006586
Healthy 6	14.25704458	-1.551162443	7.721092651	2.515988705	-4.81048818
Healthy 7	-17.06883715	-47.4640995	12.7425704	49.08339527	22.40909552
Healthy 8	32.22500384	5.639611474	50.78182974	52.47563767	68.44616124
Healthy 9	3.586033351	13.03474053	9.941500755	10.89922269	-24.40573803
Healthy 10	30.72936669	-38.11190726	59.3121698	14.62091687	-4.69290314
Healthy 11	-44.93312881	-53.35819031	-5.048521548	18.01463343	14.47683927
Healthy 12	26.58676212	-21.17075586	-58.02828417	-66.38335736	-14.92494257
TBI 1	-20.51693811	12.20695267	-20.29159756	-9.118587396	-9.918787143
TBI 2	-61.05074597	-25.08256631	16.04369124	3.960680565	-11.1074271
TBI 3	11.65703577	41.68409335	6.266057562	-33.54101521	7.09326447

TABLE 8: Max power spectrum densities (PSDs) in units of uM^2/Hz of the non-TBI trials and TBI trials during HUT and the Rest position.

Study Group & Elevation	Max PSD Slow-1	Max PSD Slow-2	Max PSD Slow-3	Max PSD Slow-4	Max PSD Slow-5
non-TBI HUT	0.077168404	0.019917619	0.195294504	0.051544805	0.010951164
TBI HUT	0.063610573	0.033597326	0.114551881	0.032000435	0.008304401
non-TBI Rest	0.077709104	0.024022726	0.162067396	0.046224266	0.010328996
TBI Rest	0.089703496	0.031006675	0.125818884	0.035344949	0.009073729